




Determination of elastic parameters of lipid membranes from simulation under varied external pressure

Maksim A. Kalutskii ^{1,2}, Timur R. Galimzyanov ^{1,2} and Konstantin V. Pinigin ^{1,*}

¹*A.N. Frumkin Institute of Physical Chemistry and Electrochemistry, Russian Academy of Sciences, 31/4 Leninsky Prospekt, Moscow 119071, Russia*

²*Department of Theoretical Physics and Quantum Technologies, National University of Science and Technology "MISiS," 4 Leninsky Prospekt, 119049 Moscow, Russia*



(Received 19 August 2022; accepted 27 January 2023; published 21 February 2023)

Many cellular processes such as endocytosis, exocytosis, and vesicle trafficking involve membrane deformations, which can be analyzed in the framework of the elastic theories of lipid membranes. These models operate with phenomenological elastic parameters. A connection between these parameters and the internal structure of lipid membranes can be provided by three-dimensional (3D) elastic theories. Considering a membrane as a 3D layer, Campelo *et al.* [F. Campelo *et al.*, *Adv. Colloid Interface Sci.* **208**, 25 (2014)] developed a theoretical basis for the calculation of elastic parameters. In this work we generalize and improve this approach by considering a more general condition of global incompressibility instead of local incompressibility. Crucially, we find an important correction to the theory of Campelo *et al.*, which if not taken into account leads to a significant miscalculation of elastic parameters. With the total volume conservation taken into account, we derive an expression for the local Poisson's ratio, which determines how the local volume changes upon stretching and permits a more precise determination of elastic parameters. Also, we substantially simplify the procedure by calculating the derivatives of the moments of the local tension with respect to stretching instead of calculating the local stretching modulus. We obtain a relation between the Gaussian curvature modulus as a function of stretching and the bending modulus, showing that these two elastic parameters are not independent, as was previously assumed. The proposed algorithm is applied to membranes composed of pure dipalmitoylphosphatidylcholine (DPPC), dioleoylphosphatidylcholine (DOPC), and their mixture. The following elastic parameters of these systems are obtained: the monolayer bending and stretching moduli, spontaneous curvature, neutral surface position, and local Poisson's ratio. It is shown that the bending modulus of the DPPC/DOPC mixture follows a more complex trend than predicted by the classical Reuss averaging, which is often employed in theoretical frameworks.

DOI: [10.1103/PhysRevE.107.024414](https://doi.org/10.1103/PhysRevE.107.024414)

I. INTRODUCTION

The shape of lipid membranes of living cells changes during a variety of cell processes: exo- and endocytosis, vesicle trafficking, assembly of viruses, embedding of proteins, etc. [1]. Membrane reshaping is controlled by the energetic cost of involved deformations, for which the theory of elasticity is often employed [2–12]. The Helfrich model, one of the most influential continuous theories in the field of lipid membranes, considers a lipid membrane as a structureless thin fluid film. Mathematically, this film can be modeled as a two-dimensional (2D) surface S , the deformations of which are described by the elastic energy functional [13]

$$w = \int_S \left(\frac{k}{2} (K - K_0)^2 + \bar{k} K_G \right) dS, \quad (1)$$

where $\int_S dS$ is the integration over S , K is the extrinsic curvature, K_G is the Gaussian curvature, K_0 is the spontaneous

curvature, k is the bending modulus, and \bar{k} is the Gaussian curvature modulus.

The scope of the Helfrich model is limited by macroscopic length scales that are much larger than the thickness of lipid bilayers. More elaborate theories are used to take into account more microscopic deformations [4,11,12,14–17]. These models take into account the inner structure of lipid bilayers, omitted in the Helfrich model. Detailed 2D elasticity models extend their application to each lipid monolayer and introduce an additional internal degree of freedom, the so-called tilt deformation. This deformation describes the deviation of lipid tails from the normal to a monolayer surface. Consideration of a lipid membrane at a microscale not only is of fundamental interest *per se* but also provides tools for describing the processes occurring at the microscale: stalk formation during membrane fusion [2,6], fission [3,18], pore formation [9,10], membrane-mediated interaction between membrane inclusions (membrane proteins, antimicrobial peptides, and regulatory lipids) [12,17,19–25], or structure of the interface boundary between different membrane phases [4,26]. An alternative approach to taking into account the internal structure of lipid membranes is to use the classical theory of elasticity and describe lipid bilayers as elastic plates of finite thickness.

*Author to whom all correspondence should be addressed: piniginkv@gmail.com

These models enable a detailed description of lipid-protein interactions [27–29]. Microscopic theories are also used to develop and refine the corresponding 2D models: For example, the model of Hamm and Kozlov [14] is based on the classical 3D theory of elasticity. Recently, the classical 3D theory of elasticity shed light on the nature of the tilt-curvature coupling in lipid membranes [15–17]; the importance of the curvature gradient contribution to the elastic energy was also emphasized [17]. It was also shown that the Gaussian curvature term in the elastic energy leads to membrane instability when the tilt degree of freedom is taken into account [17].

Another advantage of considering lipid membranes as a 3D elastic medium is that it permits the calculation of elastic parameters for phenomenological models. A major set of elastic parameters, such as membrane stretching modulus, bending modulus, spontaneous curvature, and position of the neutral surface, can be calculated from the local stretching modulus $E(z)$ [14,15,17,30], where z is the coordinate along the membrane thickness. In this work we show that an important mechanical property, the local Poisson's ratio $\nu(z)$, can be obtained using the microscopic elastic theory. Both $E(z)$ and $\nu(z)$ can be characterized by the response of local stresses distributed inside a lipid membrane to changes in external pressure. While the local stretching modulus can be derived from the stress profiles (pressure profile with a negative sign) obtained under different surface tensions [31], we show in this work that the local Poisson's ratio can be derived as a response of the stress profile to a change in isotropic ambient pressure. Since the stress profile calculation is a routine task in molecular-dynamics (MD) simulations, the microscopic theory provides a straightforward way of calculating elastic parameters *in silico*.

Despite the presence of the theoretical basis for calculating elastic parameters from the stress profiles, only one elastic parameter is determined this way, the monolayer spontaneous curvature. The method is based on the calculation of the first moment of the stress profile, which gives the product of the bending modulus and spontaneous curvature of a lipid monolayer. Therefore, to measure the spontaneous curvature, it is necessary to know the value of the bending modulus, which is usually obtained from simulations or experiments in some other way [32–35]. One of the most popular *in silico* methods for the measurement of the bending modulus is the spectral analysis of membrane undulations. This method relies on monitoring fluctuations [15,16,34,36–43] of either a membrane surface or the orientation of individual lipids, called directors. Although this method is quite accurate and requires the simulation of systems of moderate size [41,42], it has mainly been applied to single-component systems. The consideration of lipid mixtures demands assumptions, the validity of which is rather vague, such as an analog of the Reuss averaging employed in Ref. [36] for the bending modulus. In addition, a recent comprehensive study [43] shows that ambiguity in the definitions of membrane surfaces and directors leads to substantial systematic errors that can reach 40% (according to row 2 of Fig. 5 in Ref. [43]). Another popular method for determining the bending modulus is based on membrane buckling [44,45]. Although this approach has the advantage of not assuming any microscopic underpinning of the Helfrich Hamiltonian, the composition-curvature

coupling effect [46,47] makes this method inapplicable to multicomponent lipid membranes. All existing methods for the determination of membrane elastic parameters usually focus on only one elastic parameter. Therefore, a complete analysis of the mechanical properties of lipid membranes requires several different analyses and simulations. Contrary to this, the stress profile approach provides all the major elastic parameters in one method, thereby significantly simplifying the procedure.

Here we propose an *in silico* method for the determination of membrane elastic parameters based on the calculation of the lateral stress profiles of planar bilayers obtained at various external pressures. This method relies on a fundamental physical characteristic of membrane material, the local stress, and lacks the ambiguity of the fluctuations-based methods. Also, the planar configuration ensures that the curvature and lipid composition are not coupled as in approaches using nonplanar configurations such as the buckling procedure. The only requirement for the proposed method is a proper sampling of local stresses, which is usually easy to achieve in MD simulations. It enables studying not only lipid mixtures but also potentially other lipid systems, such as monolayers in contact with water and oil, membranes with embedded proteins, or other adsorbed molecules.

The first attempt to relate the elastic parameters to the stress profile was made in Ref. [31]. Although the authors provided a basic theoretical framework for determining membrane elastic moduli, neither error analysis nor explicit values of the elastic parameters were provided. Here we revise and generalize the approach of Campelo *et al.* [31]. We provide an important correction to the expression for the local stretching modulus $E(z)$ derived in Ref. [31]. We show that with this correction the method provides values of the elastic moduli that coincide with the experimental values, which otherwise deviate significantly. We consider a more general condition of global incompressibility, which is supported by both experiments [48–51] and MD simulations [52]. Taking into account global incompressibility, we derive the stress-strain relation of planar bilayer membranes by performing the variation of the most general classical elastic energy functional. From this stress-strain relation, we derive an expression for the local Poisson's ratio of lipid membranes, providing a method for calculating the local Poisson's ratio solely from a stress profile.

Based on the revised microscopic elastic theory, we establish a computational protocol for the calculation of lipid bilayer elastic parameters. We greatly simplify the approach presented in Ref. [31] by calculating monolayer elastic parameters as derivatives of the moments of the local tension profile with respect to stretching, instead of using the local stretching modulus. We apply this protocol to Martini dioleoylphosphatidylcholine (DOPC), dipalmitoylphosphatidylcholine (DPPC), and their mixture to obtain the following elastic parameters of these systems: the monolayer bending and stretching moduli, spontaneous curvature, neutral surface position, and local Poisson's ratio.

The paper is organized as follows. In Sec. II we introduce basic theoretical assumptions. In Sec. III theoretical results are presented. In the next two sections we focus on the application of the theoretical results to the determination of lipid membrane elastic parameters from MD simulations. In Sec. IV we

describe the proposed methodology. In Sec. V the results of MD simulations are presented. In Sec. VI we summarize and discuss the results of the paper.

II. THEORY

A. Basic assumptions

We consider the monolayers of a lipid membrane as a continuous elastic medium. Our aim is to examine the forces arising in this medium due to deformations and relate them to the mechanical work required for stretching and bending, thus inferring the corresponding elastic parameters. We make the following assumptions about each monolayer: (i) lateral fluidity, (ii) transverse isotropy, (iii) positivity of the isothermal local volumetric compressibility, and (iv) volumetric incompressibility. The first two assumptions are a consequence of the fact that in a planar lipid membrane lipids can freely diffuse in the lateral direction, which leads to the isotropy of the monolayers in each plane lying parallel to the membrane, i.e., the monolayers are symmetric around the axis perpendicular to these planes. Note that lipid membranes can exist in different phases [53]. In this work we consider only the lamellar liquid crystalline phase L_α , which is biologically most relevant [54] and for which the first two assumptions hold. In other phases, such as the gel phase, both lateral fluidity and transverse isotropy can be absent due to lipid tilt [53,55]. The third assumption concerns the classicality of the material under consideration, since materials with negative compressibility, the volume of which expands in response to increasing pressure, are rare and do not include lipid membranes [56]. The fourth assumption follows from experiments [48–51] and simulations [57,58], showing that the global bulk modulus of lipid membranes is close to that of water, which is 2.2 GPa at 25 °C and 0 bar [59]. This is a quite large value in comparison with other elastic moduli of lipid membranes, scaled to the appropriate units. Let us consider, for example, the stretching deformation mode, at which the area per lipid increases by $1 + \alpha$. The energetic cost of this deformation is equal to $w_A = \frac{1}{2}k_{A,m}\alpha^2A$, where A is the surface area of the considered monolayer patch and $k_{A,m}$ is the monolayer stretching modulus. If we suppose that this deformation is realized due to a volume change, the energy cost would be $w_V = \frac{1}{2}k_V\alpha_V^2V$, where V is the volume of the monolayer patch and α_V indicates the increase in volume by $1 + \alpha_V$. If the monolayer thickness remains constant, then $\alpha_V = \alpha$ and we can write $\frac{w_V}{w_A} = \frac{k_VV}{k_{A,m}A} = \frac{k_Vh}{k_{A,m}}$, where h is the monolayer thickness and $V = hA$. For $k_V = 2.2 \text{ GPa} \approx 530 k_B T \text{ nm}^{-3}$ (k_B is the Boltzmann constant and $T = 300 \text{ K}$), $k_{A,m} \approx 30 k_B T \text{ nm}^{-2}$ [60], and $h \approx 2 \text{ nm}$ [60], we obtain $\frac{w_V}{w_A} \approx 35 \gg 1$, implying that the elastic energy of the volume change is negligible upon stretching. It is of note that two types of volumetric incompressibility can be considered: local incompressibility and global incompressibility. Local incompressibility implies that every local volume element does not change during deformations. Although local incompressibility implies global incompressibility, the converse, in general, is not true. In experiments [48–51], due to precision restraints, it is difficult to measure the local bulk modulus, and therefore only the global bulk modulus is known. In Ref. [48], for instance, the

volume of 70:30 dimyristoylphosphatidylcholine/cholesterol multilayers was investigated at high pressures. To do this, the average area per lipid and monolayer thickness were measured by neutron diffraction. From these data, only the total volume per lipid could be calculated, from which the global isothermal compressibility (inverse of the bulk modulus) was determined to be $(0.1\text{--}0.6) \times 10^{-4} \text{ bar}^{-1}$. Thus, in this work, we will assume global incompressibility, which is a more general condition than local incompressibility and is supported by experiments.

Let us consider the elastic energy of lipid monolayers. We will analyze only deformations of stretching and pure bending whereby lipid molecules do not tilt. From the lateral fluidity and transverse isotropy, it follows that planar monolayers have only two variables, which describe deformations: (i) lateral stretching ε , i.e., the relative increase in the local area per lipid $\varepsilon \equiv \frac{A_1 - A_0}{A_0}$, where A_0 is the initial surface area and A_1 is the surface area of the deformed state, and (ii) longitudinal stretching ε_\perp along the axis perpendicular to the plane of isotropy, given as $\varepsilon_\perp = \nabla_z \zeta(z) - 1$, where $\zeta(z)$ is a z -dependent thickness of a deformed state with z the coordinate along the longitudinal direction. Note, however, that since we also have the assumptions of global incompressibility and positivity of the local bulk modulus, ε and ε_\perp are not independent. Indeed, let us consider a lipid monolayer under some uniform stretching ε . In this case, the thickness of the monolayer is completely determined by ε due to global incompressibility. Now let us fix this thickness and start to apply higher pressure to the sides of the monolayer. Suppose that during this procedure longitudinal stretching $\tilde{\varepsilon}_\perp$, counted relative to the state before applying the higher pressure, becomes nonzero. This would imply that at some point $\tilde{\varepsilon}_\perp > 0$, as the total thickness is fixed. This in turn implies that at this point the local volume would increase in response to an increase in the external pressure, which, however, contradicts the assumption of the positivity of the bulk modulus. Therefore, ε_\perp is a definite function at every ε . Note that this is true for uniform stretching, but might not be valid for bending. However, any deviations from the flat-state relation between ε_\perp and ε can be assumed to be small and neglected in accordance with the classical theory of elastic plates [61].

B. Elastic energy and parameters

Since ε and ε_\perp are not independent, the elastic energy density W of a lipid monolayer can be written as a function of only ε . We attribute this density to the initial state, in which the monolayer is flat, writing the total elastic energy as $\int_{V_0} W dV$, where V_0 is the initial volume occupied by the monolayer. Let us introduce a Cartesian coordinate system xyz , the z axis of which coincides with the axis of symmetry and points from the hydrophilic to the hydrophobic part of the monolayer. Using this coordinate system, we can write the Taylor series of the elastic energy

$$W(\varepsilon(z), z) = \sigma_0(z)\varepsilon(z) + \frac{1}{2}E(z)\varepsilon(z)^2 + \dots, \quad (2)$$

where the elastic parameters σ_0 and E depend only on z due to the lateral symmetry of the monolayer. It should be noted that both σ_0 and E correspond to the quantities averaged over a sufficiently long time, for at any instant of time σ_0 and E

can depend on x and y , as the configuration of lipid molecules along the xy plane can be different. In general, the local stretching ε may also depend on x and y , but in the following we will be interested only in the deformations with constant ε along the x and y axes. The function $E(z)$, responsible for the quadratic contribution in ε , is the local stretching modulus, while $\sigma_0(z)$ corresponds to the preexisting stress at $\varepsilon = 0$.

For each deformation, it is necessary to consider the compressibility condition

$$\beta(\varepsilon, z) \equiv (1 + \varepsilon(z))(1 + \varepsilon_z(\varepsilon, z)), \quad (3)$$

where $\beta(\varepsilon)$, which we will call the volume factor, is the ratio of the deformed local volume to the initial local volume. Since $\beta(\varepsilon, z) \rightarrow 1$ as $\varepsilon \rightarrow 0$, we can employ the results for the elastic constants, previously obtained under the incompressibility assumption in Refs. [14,15,17],

$$k_{A,m} = \int_{m_0} E(z) dz, \quad (4a)$$

$$z_0 = \frac{1}{k_A} \int_{m_0} E(z) z dz, \quad (4b)$$

$$k_m = \int_{m_0} E(z) (z - z_0)^2 dz, \quad (4c)$$

$$K_{0,m} = \frac{1}{k_m} \int_{m_0} \sigma_0(z) z dz, \quad (4d)$$

where \int_{m_0} denotes integration over the thickness of the monolayer in the initial state, $k_{A,m}$ is the monolayer stretching modulus, z_0 is the location of the neutral surface, k_m is the monolayer bending modulus relative to the neutral surface, and $K_{0,m}$ is the monolayer spontaneous curvature. Note that in Eqs. (4a)–(4d) the limits of integration range over not only the lipid material but also the adjacent layer of water molecules, which are involved in the structure of a lipid bilayer. Therefore, lipid-water interactions are taken into account in Eqs. (4a)–(4d). In general, the monolayer bending modulus relative to an arbitrary plane parallel to the monolayer is given by the expression $\tilde{k}_m = \int E(z) (z - \tilde{z})^2 dz$, where \tilde{z} is the coordinate of the chosen plane [14,17]. A plane, relative to which the bending modulus is minimal, is called the neutral surface. The location of the neutral surface, given in Eq. (4b), follows from the equation $\partial \tilde{k}_m / \partial \tilde{z} = 0$. The bending modulus relative to the neutral surface is of the highest interest since bending relative to this plane corresponds to the easiest way to bend the monolayer.

III. THEORETICAL RESULTS

A. Local tension

In this section we provide a theoretical framework for the determination of the elastic parameters given in Eqs. (4a)–(4d). To calculate the integrals in Eqs. (4a)–(4d), we suggest the following consideration. From Eq. (2) it follows that $E(z) = \frac{\partial^2 W(\varepsilon, z)}{\partial \varepsilon^2} \Big|_{\varepsilon=0}$. The latter equality can be rewritten as $E(z) = \frac{\partial \sigma(\varepsilon, z)}{\partial \varepsilon} \Big|_{\varepsilon=0}$, where $\sigma(\varepsilon, z) \equiv \frac{\partial W(\varepsilon, z)}{\partial \varepsilon}$. The quantity $\sigma_L(\varepsilon) \equiv \int_{m_0} \sigma(\varepsilon, z) dz$ is the lateral tension at stretching ε [62], for $\sigma_L(\varepsilon)$ and $A_0 \varepsilon$ represent the conjugate pair for the elastic energy $A_0 \int W(\varepsilon, z) dz$, where A_0 is the surface area

of the reference state. It is therefore natural to call $\sigma(\varepsilon, z)$ an ε -dependent local tension or tension profile. Inserting the relation $E(z) = \frac{\partial \sigma(\varepsilon, z)}{\partial \varepsilon} \Big|_{\varepsilon=0}$ into Eqs. (4a)–(4d) and interchanging the derivative and integral signs, we obtain

$$k_{A,m} = \frac{d}{d\varepsilon} \int_{m_0} \sigma(\varepsilon, z) dz \Big|_{\varepsilon=0}, \quad (5a)$$

$$z_0 = \frac{1}{k_{A,m}} \frac{d}{d\varepsilon} \int_{m_0} \sigma(\varepsilon, z) z dz \Big|_{\varepsilon=0}, \quad (5b)$$

$$k_m = \frac{d}{d\varepsilon} \int_{m_0} \sigma(\varepsilon, z) (z - z_0)^2 dz \Big|_{\varepsilon=0}, \quad (5c)$$

$$K_{0,m} = \frac{1}{k_m} \int_{m_0} \sigma(0, z) z dz. \quad (5d)$$

To find the expression for $\sigma(\varepsilon, z)$, we perform the variation of the elastic energy with respect to ε (see Appendix A) and obtain the expression for the stress tensor, Eq. (A5). Then $\sigma(\varepsilon, z)$ can be related to the lateral part of the stress tensor as

$$\sigma(\varepsilon, z) = \frac{[S(\varepsilon, z, P_z) + P_z] \beta(\varepsilon, z)}{1 + \varepsilon} - P_z \frac{\partial \beta(\varepsilon, z)}{\partial \varepsilon}, \quad (6)$$

where P_z is the external pressure, i.e., 1 bar under normal conditions, and $S(\varepsilon, z, P_z)$ is the lateral local stress profile, i.e., the lateral part of the stress tensor. The sign convention we use in Eq. (6) is such that a negative value of $S(\varepsilon, z, P_z)$ means repulsion.

B. Scaling

In Eq. (6), the stress profile $S(\varepsilon, z, P_z)$ is given relative to the reference state at $\varepsilon = 0$, i.e., $S(\varepsilon, z(\zeta), P_z) \equiv \tilde{S}(\varepsilon, \zeta, P_z)$, where $\tilde{S}(\varepsilon, \zeta, P_z)$ and ζ are the lateral stress and coordinate along the axis of symmetry in a deformed state of the monolayer, respectively. The relation between z and ζ can be described by some scaling function $z(\zeta)$, which maps the points of the monolayer in the reference state to the corresponding points in the stretched or compressed state of the monolayer. Here z and ζ are not equal since the membrane thickness changes upon uniform stretching or compression. In the case of the local incompressibility assumption, the relation between z and ζ is $\zeta = (1 + \varepsilon)^{-1} z$, which we will call uniform scaling. In a more general case of global incompressibility, the scaling function can be found from the compressibility condition $(1 + \varepsilon) \nabla_z \zeta(\varepsilon, z) = \beta(\varepsilon, z)$,

$$\zeta(\varepsilon, z) = (1 + \varepsilon)^{-1} \int_0^z \beta(\varepsilon, t) dt, \quad (7)$$

which we refer to as exact scaling. To determine $\beta(\varepsilon, z)$, we set $\varepsilon = 0$ and take the derivative of Eq. (6) with respect to P_z at $P_z = 1$ bar and define

$$\gamma(z) \equiv \frac{\partial \beta(\varepsilon, z)}{\partial \varepsilon} \Big|_{\varepsilon=0} = \frac{\partial S(0, z, P_z)}{\partial P_z} + 1. \quad (8)$$

Thus, the derivative of $\beta(\varepsilon, z)$ is determined by the response of the lateral stress profile to changes in ambient pressure. Direct calculations from MD data show that $\beta(\varepsilon, z)$ can be approximated linearly, $\beta(\varepsilon, z) = 1 + \gamma(z)\varepsilon$, and higher-order terms in ε are negligibly small (see Sec. IV B and Appendix B).

C. Poisson's ratio

The $\gamma(z)$ also permits the determination of the local Poisson's ratio, an important parameter characterizing the deviation of material from local incompressibility. It is defined as $\nu(z) \equiv -\frac{1}{2} \lim_{\varepsilon \rightarrow 0} \frac{\varepsilon}{\varepsilon_z(z)}$ and is equal to 0.5 in the case of local incompressibility. Inserting $\varepsilon_z(z)$ from Eq. (3) into the definition of $\nu(z)$, we get

$$\nu(z) = \frac{1}{2[1 - \gamma(z)]}. \quad (9)$$

Thus $\gamma(z)$, given in Eq. (8) and which can be directly measured in MD simulations, provides information about both the local volume factor and the local Poisson's ratio. From Eq. (9) it follows that in the case of local incompressibility $\gamma(z) = 0$, which implies, according to Eq. (8), that changes in ambient pressure are evenly spread over the lateral stress profile. In general, however, $\gamma(z)$ might be different from zero, which would imply the deviation from local incompressibility.

D. Integral relations

Let us now consider what integral relations follow from Eqs. (5a) and (5c) for the stretching and bending moduli. It is convenient to introduce a local tension relative to the state corresponding to stretching ε , $\sigma_\varepsilon(\bar{\varepsilon}, \zeta) \equiv \frac{\partial \bar{W}(\bar{\varepsilon}, \zeta)}{\partial \bar{\varepsilon}}$, where $\bar{W}(\bar{\varepsilon}, \zeta) \equiv \frac{W(\varepsilon(\bar{\varepsilon}), z(\zeta))}{\beta(\varepsilon(\bar{\varepsilon}), z(\zeta))}$ and $\bar{\varepsilon}$ are the elastic energy density and stretching written relative to the stretched state, respectively. Then, using the equality $\sigma(\varepsilon, z)dz = \sigma_\varepsilon(0, \zeta)d\zeta$, from Eq. (5a) we get the classical relation $k_{A,m} = \frac{d}{d\varepsilon} \sigma(\varepsilon)|_{\varepsilon=0}$ between the stretching modulus and lateral tension at stretching ε , $\sigma(\varepsilon) \equiv \int_{m_\varepsilon} \sigma_\varepsilon(0, \zeta)d\zeta$. If we consider Eq. (5c) for the bending modulus, it can be rewritten as

$$k_m = \frac{d}{d\varepsilon} \int_{m_\varepsilon} \sigma_\varepsilon(0, \zeta)[z(\zeta) - z_0]^2 d\zeta \Big|_{\varepsilon=0}. \quad (10)$$

The integral on the right-hand side resembles the Gaussian curvature modulus [14,63,64] corresponding to finite stretching ε , $\bar{k}_m(\varepsilon) = \int_{m_\varepsilon} \sigma_\varepsilon(0, \zeta)(\zeta - \zeta_0)^2 d\zeta$. The difference is that in Eq. (10) the distance from the neutral surface is taken relative to the reference state at $\varepsilon = 0$, $z(\zeta) - z_0$ instead of $\zeta - \zeta_0$, where ζ_0 is the neutral surface position at stretching ε . In the case of local incompressibility and quadratic energy law, $z(\zeta) - z_0 = (1 + \varepsilon)(\zeta - \zeta_0)$, which turns Eq. (10) into

$$k_m = 2\bar{k}_m(0) + \frac{d}{d\varepsilon} \bar{k}_m(\varepsilon) \Big|_{\varepsilon=0}. \quad (11)$$

Thus, the dependence of the Gaussian curvature modulus on stretching contains information about the bending modulus. Below, among other things, we will test the validity of Eq. (9) and its assumptions in MD simulations.

IV. METHODS

To obtain stress profiles, we performed a coarse-grained (CG) MD simulation. We used the Martini 3 [65] force field to represent lipid bilayers. Each system consisted of 256 lipids and 11 water beads per lipid. Since in the Martini force field one water bead corresponds to four water molecules, the virtual number of water molecules per lipid is thus 44,

which is about twice the number of water molecules per lipid involved in the structure of a lipid bilayer as reported both by experiments (25) [66] and MD simulations (17) [67]. The MD simulations were run with GROMACS 2020 [68,69] program package. The long-range electrostatics was treated by the reaction field method and relative dielectric constant $\varepsilon = 15$ [32]. The cutoff for the Lennard-Jones and Coulomb interactions was set to 1.2 nm. The temperature was controlled with the velocity-rescale thermostat, which produces a correct canonical ensemble [70]. For the solvent and bilayers, two separate temperature coupling groups were introduced and the coupling constant was set to $\tau_T = 1$ ps. To control the constant surface tension, the Berendsen barostat [71] with the surface-tension coupling was employed with a time constant of 3 ps and isothermal compressibility of 3×10^{-5} Pa. For all simulations, a 20-fs time step was used. The systems were built and equilibrated using the CHARMM-GUI web server [72–74].

A. Resampling stress and grid data

Each system at each tension was simulated for 1 μ s after equilibration for 100 ns. Every 5 ps a trajectory frame was saved for subsequent analysis of the local stress. The MD simulations were performed at surface tensions of -100 , -50 , 0 , 75 , and 150 bar nm. For the statistical analysis, we divided the simulation time into 20 blocks of 50 ns each. Each block was then analyzed with GROMACS-LS [75–78] using the covariant central force decomposition (cCFD). The lateral stress was determined as an average between xx and yy components of the obtained local stress. Before the local stress calculation, the simulation box was centered with respect to the membrane center of mass. The grid step for the local stress was set to 0.05 nm. One additional point was added after the last grid point to make the lateral stress periodic. Then each stress profile was centered by subtracting the coordinate of the last grid point divided by 2 from the grid coordinates. Thus, the midplane of the membrane was at $z = 0$. After that, the stress profile of each block was symmetrized by adding the stress profile in reverse order to the initial stress profile and dividing by 2. Then, from the 20 obtained stress profiles, 20 stress profiles were randomly sampled with repetition and averaged. The latter was repeated 200 times and thus 200 stress profiles were obtained. The grid data in GROMACS-LS represent the average grid over the simulation time. Therefore, along with 200 profiles, 200 grids were obtained by averaging the corresponding grid data. To determine stretching ε , at each tension σ the lateral size of the simulation box $L(\sigma)$ was determined as the average of the lengths of the simulation box along the x axis (the instantaneous lengths along the x and y axes were equal) over the entire simulation time of 1 μ s. Then stretching was determined as $\varepsilon = L(\sigma)^2/L(0)^2 - 1$.

B. Scaling

In the case of the uniform scaling, all 200 grids of the stress profiles were divided by $1 + \varepsilon_z(\sigma)$, where $\varepsilon_z(\sigma) = L_z(\sigma)/L_z(0) - 1$, with $L_z(\sigma)$ the longitudinal size of the box, which was determined as the average size of the 200 obtained grids. The exact scaling, given by Eq. (7), requires

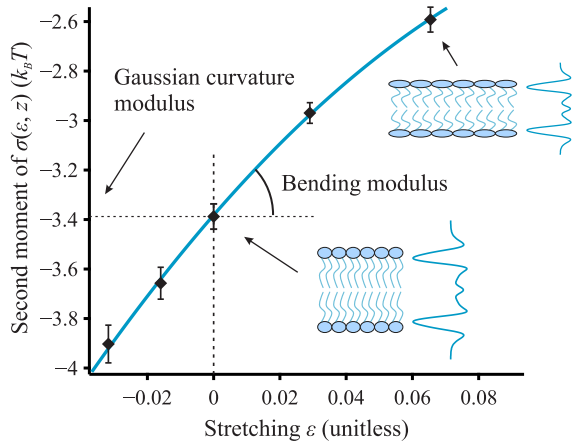


FIG. 1. Illustration of the proposed method using the example of the determination of the monolayer bending modulus of DPPC at 325 K. The horizontal axis represents stretching ε , i.e., the relative change in the surface area. The vertical axis shows the values of the second moment of the local tension $\int_{m_0} \sigma(\varepsilon, z)(z - z_0)^2 dz$, where $\sigma(\varepsilon, z)$ is the local tension and z_0 is the neutral surface position. The value of $\int_{m_0} \sigma(0, z)(z - z_0)^2 dz$ is by definition equal to the Gaussian curvature modulus, and the slope of the tangent at $\varepsilon = 0$ is equal to the monolayer bending modulus according to Eq. (5c). The two depicted lipid bilayers correspond to the tensionless and stretched states. The stretching of the upper bilayer is exaggerated for illustrative purposes. The corresponding calculated lateral stress profiles are shown to the right of the bilayers.

the calculation of $\beta(\varepsilon, z)$. For this, a linear approximation $\beta(\varepsilon, z) = 1 + \gamma(z)\varepsilon$ was employed, as it can be shown that the second derivative $\frac{\partial^2 \beta(\varepsilon, z)}{\partial \varepsilon^2} \Big|_{\varepsilon=0}$ is negligibly small (see Appendix B). To determine $\gamma(z)$, given in Eq. (8), it is necessary to apply the isotropic pressure to a membrane. To achieve this, we set the surface tension to zero and varied P_z , setting the following pressures: -50 , -25 , 1 , 25 , and 50 bar. At each P_z , the simulations were performed with the same protocol as described above. We note that, despite the global incompressibility assumption, the longitudinal size of the box may slightly change when the isotropic pressure is applied. This change, however, is rather small and in the case of, for instance, DPPC membrane does not exceed 0.2%. Nevertheless, to make the grid sizes match each other, we perform the uniform scaling in the same way as described above for the cases of nonzero tensions. Then $\frac{\partial S(0, z, P_z)}{\partial P_z} + 1$ was calculated at $P_z = 1$ bar by a linear least-squares estimator. The latter was performed 200 times for all 200 stress profiles at different P_z . Thus, 200 random values of $\gamma(z)$ were obtained. Then the Poisson's ratio and exact scaling map were found by inserting the values of $\gamma(z)$ and $\beta(\varepsilon, z) = 1 + \gamma(z)\varepsilon$ into Eqs. (9) and (7), respectively. After that, the obtained scaling maps were applied to grid data and 200 local tensions at each stretching were determined according to Eq. (6).

C. Elastic parameters

Once the local tension $\sigma(\varepsilon, z)$ is determined, we can use Eqs. (5a)–(5d) to find the elastic parameters by calculating the moments of $\sigma(\varepsilon, z)$. For this, at each ε one random local tension was selected out of 200 available. Then the stretching

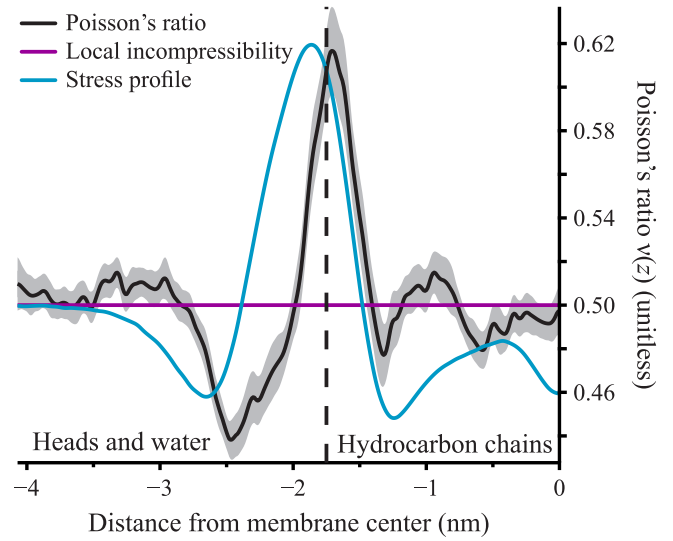


FIG. 2. Local Poisson's ratio of DPPC at 325 K as a function of distance from the center of the bilayer. The black curve and gray shading represent the mean value of the Poisson's ratio and 95% confidence band, respectively. The purple line corresponds to local incompressibility, in which case the Poisson's ratio is constant and equal to 0.5. The zero-tension stress profile, adjusted to the magnitude of the Poisson's ratio, is given in arbitrary units by the cyan curve. The dashed vertical line shows the mean coordinate of the first glycerol bead, approximately equal to -1.75 nm, indicating the boundary between the hydrophobic and hydrophilic parts of the monolayer.

modulus, location of the neutral surface, bending modulus, and spontaneous curvature were determined consequently according to Eqs. (5a)–(5d). To find the derivatives with respect to ε , a quadratic least-squares regression was performed. This procedure was repeated multiple times to get sufficient sampling statistics. The proposed method in the case of the determination of the bending modulus is illustrated in Fig. 1.

V. SIMULATION RESULTS

In this section we present the results of the MD simulations. We start with DPPC, a widely used lipid in MD simulations. First, we find the Poisson's ratio $\nu(z)$ (Fig. 2), calculating the response $\gamma(z)$ of the lateral stress profile to the external isotropic pressure P_z according to Eq. (8) and inserting it into Eq. (9). A linear least-squares fit is used to find $\gamma(z)$, for at each z a linear function agrees well with the data within the error limits.

Figure 2 shows that at many coordinate points the Poisson's ratio differs from 0.5, i.e., from the incompressibility condition. We observe a correlation between the stress profile and Poisson's ratio: In the headgroup region, where the stress is repulsive, the Poisson's ratio is less than 0.5, implying that the magnitude of the longitudinal stretching is larger than that of the lateral stretching during deformations. By contrast, in the glycerol region ($z \approx -1.75$ nm), where the attraction occurs, the ratio is greater than 0.5 and reaches a maximum deviation from 0.5: $\nu = 0.62 \pm 0.01$. In the repulsive headgroup region, the Poisson's ratio is again smaller than 0.5.

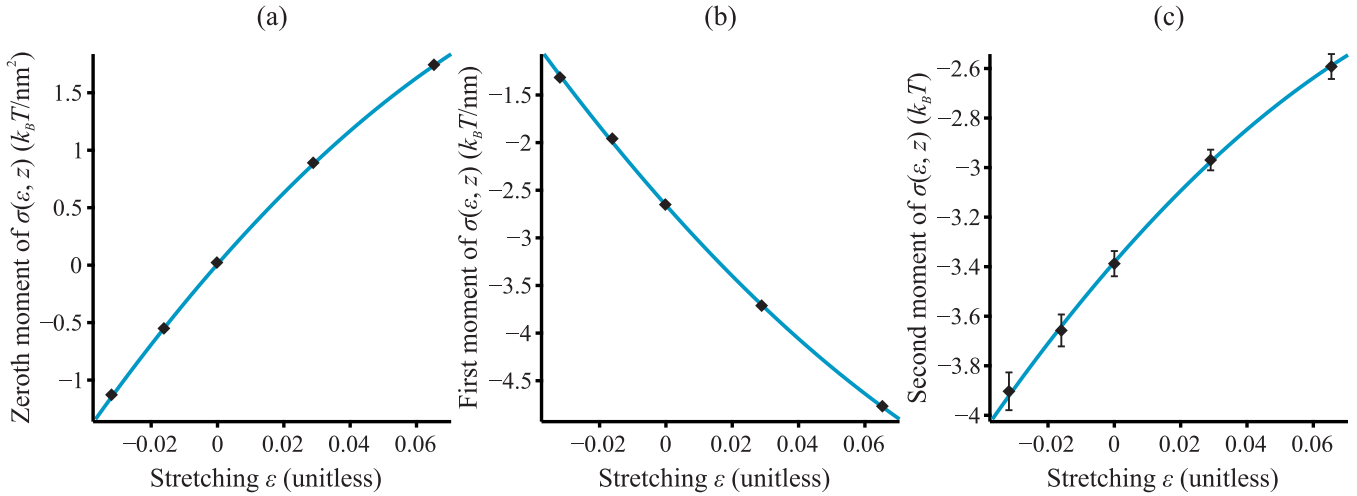


FIG. 3. (a) Zeroth moment $\int_{m_0} \sigma(\epsilon, z) dz$, (b) first moment $\int_{m_0} \sigma(\epsilon, z)(z - z_0) dz$, and (c) second moment $\int_{m_0} \sigma(\epsilon, z)(z - z_0)^2 dz$ of the local tension $\sigma(\epsilon, z)$, where z_0 is the position of the neutral surface, as functions of stretching ϵ . According to Eqs. (5a)–(5c), the tangent at $\epsilon = 0$ is equal to (a) $k_{A,m}$, (b) $k_{A,m}z_0$, and (c) k_m , where $k_{A,m}$ is the monolayer stretching modulus and k_m is the monolayer bending modulus. The cyan curves are the best-fit quadratic polynomials. The error bars in (c) indicate the standard deviation. In (a) and (b) the error bars are too small to be shown.

After the Poisson's ratio is found, we can determine the volume factor $\beta(\epsilon, z) \equiv 1 + \gamma(z)\epsilon$ and the exact scaling function (7). We employ the linear approximation of $\beta(\epsilon, z)$ because our direct calculations show that the difference between the Taylor series of $\beta(\epsilon, z)$ up to the first and second orders in ϵ is less than approximately 0.3% within the range of ϵ values considered. The moments of $\frac{\partial^2 \beta(\epsilon, z)}{\partial \epsilon^2} \Big|_{\epsilon=0}$ are also negligibly small; the details of the calculations are given in Appendix B. This allows us to use the linear approximation for $\beta(\epsilon, z)$ in the expression for the local tension (6).

To obtain the values of the local tension at different stretching, we apply the following tensions: -100 , -50 , 75 , and 150 bar nm. The absolute values of the negative tensions are chosen to be smaller, as high values might lead to a large compression of the membrane with the formation of a gel phase. The latter may occur at some critical value of compression, depending on a lipid system and temperature. Dilauroylphosphatidylcholine at 300 K, for example, transitions into a gel phase at approximately 3.8% [79]. In our simulations, the largest compression was 3.2% and we did not observe any discontinuities in the obtained data.

The stress profiles at different tensions have different end points, as the membrane thickness changes in response to uniform stretching or compression due to volumetric incompressibility. Using $\beta(\epsilon, z)$, we can determine the exact scaling function, given in Eq. (7), to map the points of the deformed membranes to the points of the initial state at zero tension. Applying this scaling map to the stress profiles, we determine the local tensions at different stretching and then find the elastic parameters as given in Eqs. (5a)–(5c). The results are shown in Fig. 3.

For each datum, to find the derivative at $\epsilon = 0$ we use least squares to approximate the data by a quadratic polynomial, as fitting with higher-order polynomials does not change the mean value within the error limits. We find

the following values for the monolayer elastic parameters: $k_{A,m} = 33.0 \pm 0.2 k_B T \text{ nm}^{-1}$, $z_0 = -1.19 \pm 0.01 \text{ nm}$, $K_{0,m} = -0.17 \pm 0.01 \text{ nm}^{-1}$, and $k_m = 15.3 \pm 0.6 k_B T$ for the monolayer stretching modulus, location of the neutral surface, spontaneous curvature, and bending modulus, respectively; the errors indicate the standard deviation. As seen in Fig. 3, the quadratic fit well describes the data; the reduced χ^2 is 2.23, 1.86, and 1.02 for the zeroth, first, and second moments, respectively. Note that, since $\sigma(0, z)$ coincides with the tension profile at zero stretching, in Figs. 3(b) and 3(c), the values at $\epsilon = 0$ are equal to $k_m K_{0,m}$ and the Gaussian curvature modulus, respectively.

Next we proceed by changing the scaling map from exact to uniform to find the corrections to the elastic parameters resulting from the deviation from local incompressibility. The results are $k_{A,m} = 32.1 \pm 0.1 k_B T \text{ nm}^{-2}$, $z_0 = -1.16 \pm 0.01 \text{ nm}$, $K_{0,m} = -0.18 \pm 0.01 \text{ nm}^{-1}$, and $k_m = 14.8 \pm 0.6 k_B T$ for the stretching modulus, position of the neutral surface, spontaneous curvature, and bending modulus, respectively. There is a slight shift in the mean values in comparison with the exact scaling. Although the discrepancy does not fall within the error limits for the stretching modulus and neutral surface, the relative deviation is less than approximately 3%. The same observation has been made for other lipid systems (DOPC and DPPC/DOPC mixture) and temperatures (see Table I).

Employing the same method, we next consider the 50:50 DPPC/DOPC lipid mixture and pure DOPC at 325 K. The results are presented in Fig. 4 and Table I. The monolayer stretching and bending moduli show opposite trends as functions of the concentration of the unsaturated lipid, DOPC: While the stretching modulus and spontaneous curvature increase with increasing DOPC concentration, the bending modulus decreases. The neutral surface position z_0 shifts towards the midplane of the membrane and varies almost linearly at the concentrations of DOPC considered. The

TABLE I. Values of the obtained monolayer elastic parameters: stretching modulus $k_{A,m}$, location of the neutral surface z_0 , spontaneous curvature $K_{0,m}$, bending modulus k_m , and the deviation of the local Poisson's ratio from the incompressibility condition $|\nu(z) - 0.5|_{\max}$. The $k_{A,m}$, z_0 , $K_{0,m}$, and k_m are determined using Eqs. (5a)–(5c) under the assumptions of local incompressibility (uniform scaling) and global incompressibility (exact scaling). The sign convention for spontaneous curvature is the following: A positive value implies that the area of the head region tends to be larger than the area of the tails. The errors indicate the standard deviation.

Parameter	DPPC $T = 325$ K		DPPC/DOPC 50:50 $T = 325$ K		DOPC $T = 325$ K		DOPC $T = 300$ K	
	Uniform scaling	Exact scaling	Uniform scaling	Exact scaling	Uniform scaling	Exact scaling	Uniform scaling	Exact scaling
$k_{A,m}(k_B T \text{ nm}^{-2})$	32.1 ± 0.1	33.0 ± 0.2	33.9 ± 0.2	35.1 ± 0.2	35.6 ± 0.1	36.5 ± 0.2	43.4 ± 0.2	44.6 ± 0.2
z_0 (nm)	-1.16 ± 0.01	-1.19 ± 0.01	-1.08 ± 0.01	-1.11 ± 0.01	-1.02 ± 0.01	-1.04 ± 0.01	-1.04 ± 0.01	-1.06 ± 0.01
$K_{0,m}$ (nm^{-1})	-0.18 ± 0.01	-0.17 ± 0.01	-0.31 ± 0.02	-0.29 ± 0.01	-0.32 ± 0.02	-0.31 ± 0.02	-0.32 ± 0.02	-0.30 ± 0.02
$k_m(k_B T)$	14.8 ± 0.6	15.3 ± 0.6	8.2 ± 0.4	9.0 ± 0.4	8.3 ± 0.6	8.7 ± 0.6	10.1 ± 0.8	10.8 ± 0.8
(pN nm)	(66.4 ± 2.7)	(68.9 ± 2.7)	(37.0 ± 2.0)	(40.2 ± 1.9)	(37.1 ± 2.5)	(39.2 ± 2.5)	(42.0 ± 3.2)	(44.8 ± 3.2)
$ \nu(z) - 0.5 _{\max}$ (unitless)		0.12 ± 0.01		0.09 ± 0.01		0.07 ± 0.01		0.08 ± 0.01

variations in the bending modulus and spontaneous curvature, however, are highly nonlinear: The difference between pure DPPC and the 50:50 mixture is much larger than the difference between the 50:50 mixture and pure DOPC. As should be expected, the bending modulus of DOPC turns out to be

smaller than that of DPPC since DOPC is an unsaturated lipid, unlike DPPC. The maximum values of the deviation of the local Poisson's ratio from the local incompressibility condition $|\nu(z) - 0.5|_{\max}$ decrease from 0.12 ± 0.01 for pure DPPC to 0.07 ± 0.01 for pure DOPC.

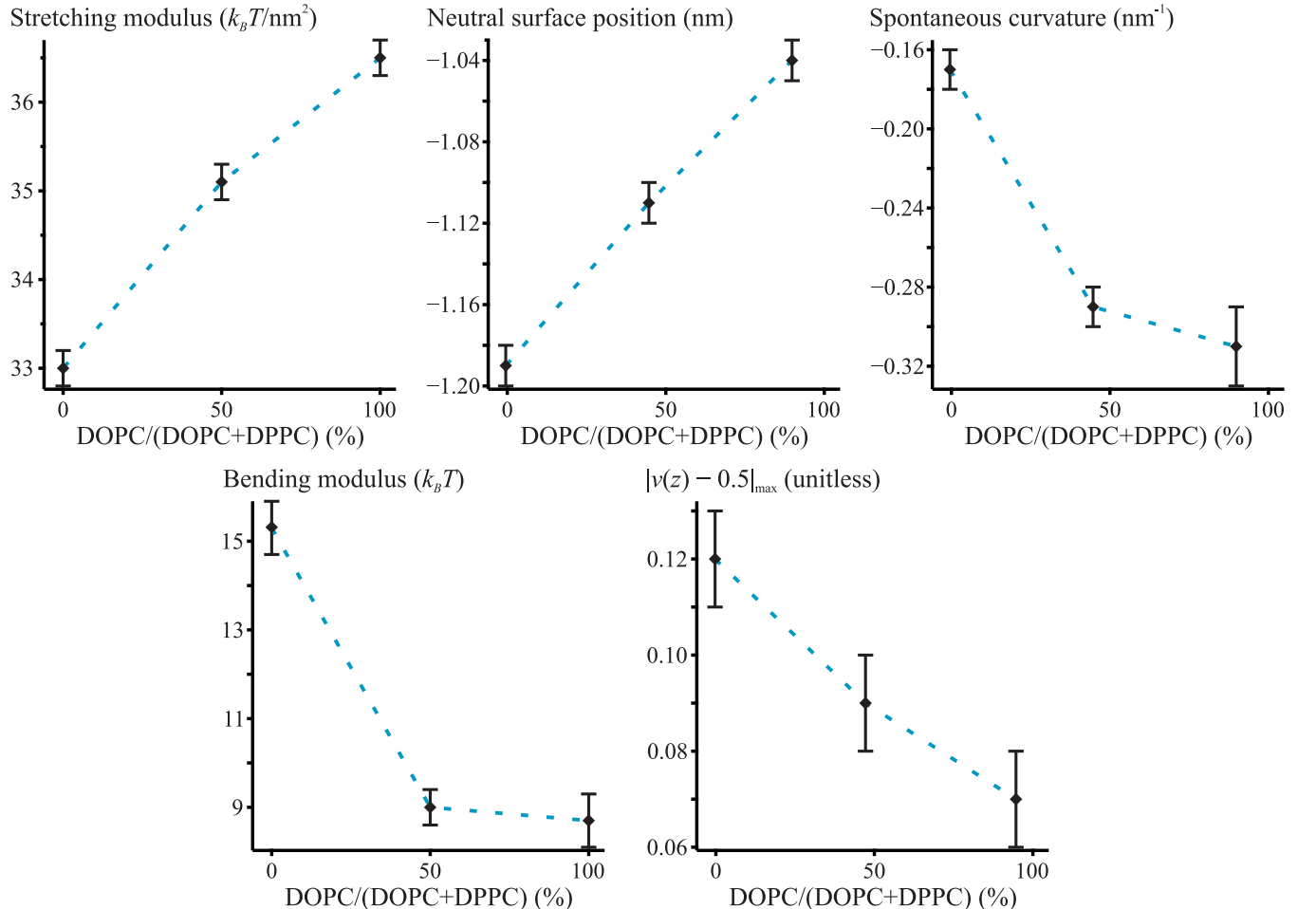


FIG. 4. Monolayer elastic parameters as functions of the DOPC concentration in the DPPC/DOPC mixture, measured using Eqs. (5a)–(5d) and (9). The error bars indicate the standard deviation.

We also simulated DOPC at 300 K to consider the dependence of the elastic parameters on temperature and to see whether the proposed method also works at smaller temperatures (Table I). The results show that as the temperature decreases, the membrane becomes more rigid: The stretching and bending moduli become larger. This is expected since the membrane gets closer to the phase transition into the gel phase as the temperature decreases. At the same time, the position of the neutral surface, spontaneous curvature, and $|\nu(z) - 0.5|_{\max}$ remain approximately constant.

In Sec. III it was shown that the bending and Gaussian curvature moduli are related by Eq. (9) under the assumptions of the quadratic energy and local incompressibility. Direct calculations for DPPC yield that the Gaussian curvature modulus is $-3.40 \pm 0.05 k_B T$ and its derivative is $14.8 \pm 2.2 k_B T$, leading to $8.1 \pm 2.2 k_B T$ for the bending modulus, which is far from the measured value $15.3 \pm 0.6 k_B T$. This implies that the assumptions of the quadratic energy law and local incompressibility are not valid, which agrees with the observation that the local Poisson's ratio deviates from the local incompressibility condition (see Fig. 2). The energy deviation from the quadratic law can also be seen from the dependence of the monolayer tension on stretching, which is not linear [see Fig. 3(a)] as it would be in the case of the quadratic energy law. Thus, the quadratic incompressible model appears to be oversimplified, at least for the CG DPPC.

VI. DISCUSSION

In this paper we revised and generalized the approach of Campelo *et al.* [31], which relies on the measurement of the local stretching modulus $E(z)$ for the determination of elastic parameters of lipid membranes. Introducing the local tension $\sigma(\varepsilon, z) \equiv \frac{\partial W(\varepsilon, z)}{\partial \varepsilon}$, we showed that the approach of Campelo *et al.* can be largely simplified, as $\sigma(\varepsilon, z)$ permits the determination of the elastic parameters with only one fit by a quadratic function according to Eqs. (5a)–(5d) and (6) instead of calculating $E(z)$. In addition, a more general assumption of global incompressibility of lipid monolayers was considered rather than the local incompressibility condition. This allowed us, after obtaining the stress-strain relation given in Eq. (A5), to derive the expression for the local Poisson's ratio, Eq. (9). From $\nu(z)$ we found the volume factor $\beta(\varepsilon, z)$, i.e., the relative change in the local volume at position z upon stretching ε . The volume factor $\beta(\varepsilon, z)$ provided the exact scaling function (7), which maps the points of stretched monolayers to the points of unstretched monolayers and allows a more precise determination of elastic parameters than the uniform scaling function corresponding to the local incompressibility assumption. We applied the theoretical results to the determination of elastic parameters of lipid membranes in MD simulations by considering CG DPPC, DOPC, and their equimolar mixture.

A. Poisson's ratio

In this paper we considered lipid membranes as 3D elastic media and obtained the expression for the stress-strain relation (A5). Previously, lipid membranes were modeled as either incompressible [12,14–17,31,34,80] or a material with independent lateral and longitudinal stretching [52]. In our work

we instead employed the global incompressibility assumption, supported by experiments [48–51], and showed that lateral stretching and longitudinal stretching are not independent. This allowed us to express the energy as being dependent only on lateral stretching and obtain the expression for the local Poisson's ratio given in Eq. (9) that characterizes the deviation from local incompressibility. Note that within the proposed framework the Poisson's ratio is fully determined by the lateral stress profiles, i.e., without any reference to the amount of material under consideration. It is however possible to determine the Poisson's ratio from the material perspective, as was done by Terzi *et al.* [52]. The latter approach depends on the definition of the amount of material, which may contain some uncertainties with, for example, the additivity of component volumes, while the local stress method relies only on the lateral stress profile.

For all systems considered, we calculated the local Poisson's ratio $\nu(z)$. Local incompressibility implies a constant Poisson's ratio of 0.5. Our calculations showed that the Poisson's ratio of the considered systems is nonuniform: It may be smaller or larger than 0.5, depending on the region considered (see Fig. 2). The maximum deviation $|\nu(z) - 0.5|_{\max}$ lies within the range of 0.57–0.62, i.e., 14%–24% away from 0.5. The deviation of $\nu(z)$ from 0.5 implies that the local volume at position z is not conserved upon membrane stretching or compression. The corresponding change of the local volume at stretching ε is given by the volume factor $\beta(\varepsilon, z) \equiv \frac{dV'(\varepsilon, z)}{dV_0(z)} = 1 + \gamma(z)\varepsilon$, where $dV_0(z)$ is the initial local volume, i.e., at $\varepsilon = 0$, while $dV'(\varepsilon, z)$ is the local volume at stretching ε , and $\gamma(z)$ can be expressed through $\nu(z)$ from Eq. (9), resulting in $\beta(\varepsilon, z) = 1 + \frac{2\nu(z)-1}{2\nu(z)}\varepsilon$. We see that if $\nu(z) = 0.5$, then $\beta(\varepsilon, z) = 1$, i.e., the local volume is conserved. In the case of DPPC (see Fig. 2), upon stretching the local volume strongly increases [$\nu(z) > 0.5$] in the glycerol region and decreases [$\nu(z) < 0.5$] in the headgroup region. Also, there is a slight variability from the local incompressibility in the region of the lipid tails.

Variations of the local volume in some membrane regions due to the deviation of the local Poisson's ratio from 0.5 may affect the properties of the lipid matrix in this position, which can have biological consequences [52]. It is known that cell membranes can contain transmembrane proteins, the activity of which is regulated by mechanical stresses. Such a regulation occurs, for example, in mechanosensitive channels [81,82]. The change in the properties of the lipid matrix in the proximity of the membrane proteins may impact the corresponding lipid-protein interactions. Thus, the local Poisson's ratio may modulate lipid-protein interactions in response to mechanical stresses, thereby regulating the activity of membrane proteins.

B. Local tension

For the determination of the elastic parameters, we used the local tension profile $\sigma(\varepsilon, z) \equiv \frac{\partial W(\varepsilon, z)}{\partial \varepsilon}$, introduced in Eq. (6), where $W(\varepsilon, z)$ is the elastic energy density. By definition, $\sigma(\varepsilon, z)$ represents the resulting effective lateral stress given in the reference state, which does work during deformations. In this regard, $\int_{m_0} \sigma(\varepsilon, z) dz$ is by definition equal to the lateral tension at the state of stretching ε . The relations between

elastic parameters and $\sigma(\varepsilon, z)$ are given in Eqs. (5a)–(5d). The bending modulus, for example, can be found as a derivative with respect to ε at $\varepsilon = 0$ of the second moment of $\sigma(\varepsilon, z)$ relative to the neutral surface position. It should be noted that there is also another way to determine elastic parameters. The tension profile is directly related to the local stretching modulus $E(z)$: By definition, $E(z) = \frac{\partial \sigma(\varepsilon, z)}{\partial \varepsilon} \Big|_{\varepsilon=0}$. Thus, $E(z)$ could have been used, according to Eqs. (4a)–(4d), without the use of $\sigma(\varepsilon, z)$. It would require, however, the determination of $E(z)$ at some specified grid distributed throughout the thickness of the monolayer. The finer the grid, the better the result for the moments of $E(z)$. As the grid step should be at least as small as the grid used in the calculation of the stress profile, which is 0.05 nm in our case, the number of grid points for the 4-nm-thick monolayer would be 80. This greatly complicates the procedure and statistical analysis since at each point of the grid it is necessary to perform data fitting to determine the derivative of the local tension. We showed though that this is a superfluous task, as the same goal can be achieved with only one fit of the tension profile moments. Actually, $E(z)$ requires too much information to be calculated: Once $E(z)$ is determined, any moment of it can be found. This information, however, is redundant for the determination of the key elastic parameters such as stretching and bending moduli, requiring only the zeroth, first, and second moments of $E(z)$ to be known [see Eqs. (4a)–(4c)]. Previously, $E(z)$ was determined by two independent methods. In Refs. [83,84] the authors analyzed fluctuations of an area per material at position z to infer $E(z)$: From the equipartition theorem, it follows that the larger the fluctuations of this area, the smaller the $E(z)$. Also, $E(z)$, in the case of Martini DOPC, was found in Ref. [31] by Campelo *et al.*, where $E(z)$ was equated with the derivative of the stress profile with respect to stretching. However, as follows from Eq. (6), even under the local incompressibility assumption, the expression for $E(z)$ is more complicated,

$$E(z) = \frac{\partial [S(\varepsilon, z) + P_z]}{\partial \varepsilon} \Big|_{\varepsilon=0} - [S(0, z) + P_z], \quad (12)$$

i.e., $E(z)$ contains not only the derivative of the stress profile $\frac{\partial [S(\varepsilon, z) + P_z]}{\partial \varepsilon} \Big|_{\varepsilon=0}$, as was derived by Campelo *et al.* [31], but also the stress itself $-[S(0, z) + P_z]$, which is comparable in magnitude to the stress derivative. This is a consequence of the change of the membrane thickness due to the applied lateral tension, which may lead to incorrect results if not taken into account. For instance, according to our calculations, the bending modulus of DPPC would be $11.3 \pm 0.6 k_B T$ instead of $14.8 \pm 0.6 k_B T$ in the case of the uniform scaling, resulting in a rather large systematic error of $24 \pm 5\%$.

C. Elastic parameters

The method proposed in this work enables the determination of the following elastic parameters: the stretching modulus, bending modulus, spontaneous curvature, neutral surface position, and local Poisson's ratio. This is a set of parameters that can be determined from the planar configuration of lipid bilayers using Eqs. (5a)–(5d). There are other elastic parameters of lipid membranes, which were not considered in this work. An important example is the tilt modulus, which characterizes the energy cost for the deviation of lipid directors from the local normal to a lipid monolayer [11–14,85–87].

In general, the tilt deformation mode also couples with the effective extrinsic curvature and curvature gradient, which gives rise to the corresponding elastic moduli [15–17]. Other major examples include the tilt-stretching coupling modulus [17], stretching-curvature coupling modulus [17], splay modulus of individual lipid tails [88,89], and twist modulus [14]. In some theoretical frameworks, also an in-plane nematic ordering is considered, described by the Frank Hamiltonian with the corresponding elastic parameters [90–93]. This nematic ordering may stem from the presence of chiral components such as cardiolipin [91,92] in lipid membranes. In this work we considered only those elastic parameters that can be determined from pure stretching of planar lipid bilayers. Although the planar configuration of lipid membranes is quite simple, it also appears to be highly informative, as it permits the determination of the important set of elastic parameters, which are frequently employed in both 2D and 3D formulations of elastic theories of lipid membranes.

As CG systems were considered in this paper, we should not anticipate a full coincidence of the obtained elastic parameters with experimental results. In the Martini model [65], employed in this work, DPPC is represented by 12 beads, whereas real DPPC molecules consist of 130 atoms. Another simplification is the treatment of the long-range electrostatics, for which the reaction field method is used with the relative dielectric constant $\varepsilon = 15$, which is assumed to be spatially uniform [32]. In general, however, ε can be a space-dependent function [94,95]. Nevertheless, the parameters of the Martini model as well as other CG models are carefully tuned to ensure the correspondence between the physical properties of simulated and real systems [32,65]. In turn, different experimental methods may also disagree with each other. The analysis of thermal shape fluctuations of vesicles at 322 K, for example, leads to $18.4 \pm 1.1 k_B T$ for the monolayer bending modulus of DPPC [96], while the x-ray scattering at 323 K yields $14.4 \pm 2.3 k_B T$ [97]. Nevertheless, the value obtained in this work, $15.3 \pm 0.6 k_B T$ at 325 K, is quite close to these experimental results. The same is also true for the obtained values of the bending modulus of DOPC, $8.7 \pm 0.6 k_B T$ at 325 K and $10.8 \pm 0.8 k_B T$ at 300 K, and corresponding experimental results [$10.6 \pm 1.2 k_B T$ at 291 K [60], $7.5 \pm 1.5 k_B T$ at 295 K [98], and $9.7 \pm 0.4 k_B T$ at 303 K [97]]. The values of the stretching moduli are also typical [99,100]. The neutral surface of the considered systems is located at a distance of approximately 1 nm from the midplane, i.e., approximately in the middle of the lipid tail region. This is in agreement with previous simulations based on the analysis of fluctuations [34]. What is noticeable is that the obtained values of spontaneous curvature are large and negative (see Table I). In contrast, the experimental values are 0.05 ± 0.05 and $-0.04 \pm 0.04 \text{ nm}^{-1}$ for DPPC and DOPC, respectively [101]. This might be an artifact of the Martini force field, which leads to the large repulsion in the region of lipid tails (see Fig. 2), while in all-atom (AA) systems this repulsion is smaller [75]. The consequence of this may be an increase in the line tension of the membrane edge and therefore a high cost of pore formation, which is a known drawback of Martini lipids [102].

Since the proposed method applies not only to single-component membranes but also to multicomponent lipid

membranes, we analyzed the dependence of elastic parameters on the concentration of DPPC and DOPC. In general, the bending deformation entails a redistribution of lipid molecules due to the composition-curvature coupling effect [46,47]: Lipids with nonzero spontaneous curvature $K_{0,m}$ would tend to accumulate at membrane regions whose extrinsic curvature K is close to the spontaneous curvature of these lipids, relaxing the bending energy $\frac{1}{2}k_m(K - K_{0,m})^2$. This redistribution of lipids leads to a position-dependent bending modulus and spontaneous curvature $k_m = k_m(\mathbf{r})$ and $K_{0,m} = K_{0,m}(\mathbf{r})$, respectively, where \mathbf{r} is the position vector. At each \mathbf{r} , there is a specific lipid composition, and $k_m(\mathbf{r})$ and $K_{0,m}(\mathbf{r})$ mean the intrinsic (with no redistribution of lipids) bending modulus and spontaneous curvature, respectively. The method proposed in the present work considers only planar bilayers and the redistribution of lipids does not take place. Therefore, the bending moduli and spontaneous curvatures obtained in this work for lipid mixtures are intrinsic bending moduli and spontaneous curvatures. The redistribution of lipids during bending can be observed in experiments with lipid tubes [47]. In this case of lipid redistribution, a system can be characterized by an effective bending modulus that is less than the intrinsic bending modulus. Such a decrease in the bending modulus can be up to approximately 30%, and there are theoretical models that estimate this decrease from the properties of the reservoir and concentration dependence of the intrinsic elastic parameters of considered lipid mixtures [47].

In this work we considered the 50:50 DPPC/DOPC lipid mixture. While the stretching modulus of this mixture turned out to be somewhere in the between those of pure DPPC and DOPC, the bending modulus and spontaneous curvature are close to pure DOPC. Thus, the trend for the latter two parameters is highly nonlinear. The spontaneous curvature is usually assumed to be additive in experiments [101,103,104], i.e., the spontaneous curvature c_{mix} of a multicomponent lipid monolayer is assumed to be $c_{\text{mix}} = \sum_i \varphi_i c_i$, where φ_i is the mole fraction of lipids of type i and c_i is the spontaneous curvature of a single-component monolayer composed of lipids of type i . In Ref. [105] the authors considered the first moment of the stress profile, which is equal to $k_m K_{0,m}$, and showed that the spontaneous curvature of sphingomyelin and cholesterol is nonadditive. In our case, the first moment values are quite similar: $2.65 \pm 0.03 k_B T \text{ nm}^{-1}$, $2.59 \pm 0.01 k_B T \text{ nm}^{-1}$, and $2.66 \pm 0.01 k_B T \text{ nm}^{-1}$ for pure DPPC, 50:50 DPPC/DOPC, and pure DOPC, respectively. Although there is a slight nonlinearity in these values, the direct concentration dependence of the bending modulus and spontaneous curvature, given in Fig. 4, cannot be obtained within the approach of Ref. [105], as it considers only the product between the bending modulus and spontaneous curvature. The inverse of the bending modulus also does not abide by a linear trend, known as the Reuss averaging [106], sometimes used in theoretical frameworks [107,108]. According to this averaging, the bending modulus k_{mix} of a binary lipid mixture with the bending moduli k_1 and k_2 and areas per lipid a_1 and a_2 of the corresponding single-component membranes can be expressed as

$$k_{\text{mix}} = (a_1 N_1 + a_2 N_2) \left(\frac{a_1 N_1}{k_1} + \frac{a_2 N_2}{k_2} \right)^{-1}, \quad (13)$$

where N_1 and N_2 are the numbers of lipids in the mixture. Substituting into k_{mix} the areas per lipid of pure DPPC and DOPC membranes, 0.6 and 0.69 nm², respectively, and the obtained values of the bending moduli, we get $10.9 \pm 0.5 k_B T$ for the bending modulus of the 50:50 DPPC/DOPC mixture, which differs from the measured value, $9.0 \pm 0.4 k_B T$, by 21 ± 8%. Thus, the concentration dependence of the monolayer bending modulus of the considered DPPC/DOPC mixture is more complex than the classical Reuss averaging predicts. It is known that lipid membranes of living cells are usually multicomponent [54,109]. Since elastic parameters of lipid membranes determine important characteristics of various phenomena associated with membrane deformations such as energy barriers and characteristic times, the analysis of elastic parameters of multicomponent lipid membranes is of particular interest from a biological point of view to understand how living cells can regulate these phenomena by changing the lipid composition of their membranes.

The expression obtained for the local tension (6) allowed us to consider the relation between the bending modulus and moments of the stress profile. This analysis is analogous to the derivation of the classical relation between the stretching modulus and lateral tension: $k_A = \frac{d}{d\varepsilon} \sigma(\varepsilon)|_{\varepsilon=0}$. We showed that in the case of the quadratic energy law and local incompressibility the bending modulus is associated with the ε -dependent Gaussian curvature modulus according to Eq. (11). This is a consequence of the fact that the expression for the bending modulus (5c) contains the second moment of the stress profile. Our analysis showed that Eq. (11) does not hold for DPPC: k_m calculated from Eq. (11), $8.1 \pm 2.2 k_B T$, is approximately half the actual value $15.3 \pm 0.6 k_B T$. This implies that the simplifying assumption of the quadratic energy law and local incompressibility does not apply to Martini DPPC. It might seem striking that the two elastic moduli, the bending modulus and the Gaussian curvature modulus as a function of stretching, at least in the case of the quadratic energy law and local incompressibility, are not independent of each other. However, it was previously shown that the second moment of the stress profile, which is usually associated with the Gaussian curvature modulus [14,63,64], should not be considered a separate elastic modulus; rather, this term is connected with the spontaneous Gaussian curvature [17]. It should be noted that a reformulation of the Helfrich Hamiltonian exists [110]. In Ref. [110] it was proposed that it is more reasonable to replace the Gaussian curvature term with the deviatoric bending, i.e., to replace $K_G = c_1 c_2$ by $\frac{k_d}{2} (|c_1 - c_2| - \vartheta)^2$, where c_1 and c_2 are the principal curvatures, k_d is the deviatoric curvature modulus and ϑ is the spontaneous warp. This deviatoric energy contribution is written in analogy to the first term of the Helfrich Hamiltonian, $\frac{k}{2} (c_1 + c_2 - K_0)^2$ [see Eq. (1)], where $c_1 + c_2 = K$ by definition. Using the extrinsic curvature and the curvature deviator instead of the extrinsic and Gaussian curvature in the expression for the elastic energy leads to a different understanding of the membrane fusion and fission processes [111–113]. The deviatoric bending is also employed for the description of anisotropic membrane inclusions [114,115].

It should be mentioned that the second moment of the stress profile may not be the only contribution to the Gaussian curvature modulus. In Refs. [14,116] it was shown that the local

lateral shear modulus $\lambda_{LS}(z)$ also contributes to the Gaussian curvature modulus [see also Eq. (11.6) of Ref. [61]]. As in the lateral direction lipid membranes are fluid, in Ref. [14] two kinds of lateral fluidity conditions were considered, $\lambda_{LS}(z) = 0$ and $\int \lambda_{LS}(z) dz = 0$, corresponding to the local fluidity assumption and global fluidity assumption, respectively. In Ref. [17] it was shown that local fluidity follows from global fluidity due to the membrane stability requirements and thus the two assumptions are equivalent. However, the analysis of transverse fluctuations of lipid molecules shows that the twist modulus, which according to the elastic theory equals $2 \int \lambda_{LS}(z) z^2 dz$, is nonzero [41], which contradicts the equality $\lambda_{LS}(z) = 0$. On the other hand, the analysis of longitudinal fluctuations of lipid molecules shows that the curvature gradient modulus is equal to zero, which contradicts the membrane stability requirements and leads to unphysical results [17], implying that the analysis of lipid fluctuations within the elastic theory of lipid membranes is rather problematic.

It should be mentioned that there are other relations, different from Eq. (11), between the bending modulus and Gaussian curvature modulus, which were obtained in other theoretical frameworks. The classical relation, valid for isotropic elastic plates with the Poisson's ratio ν , is [61]

$$\frac{\bar{k}}{k} = \nu - 1. \quad (14)$$

The applicability of Eq. (14) to lipid membranes is rather vague. First, lipid membranes are transversely isotropic rather than simply isotropic. Second, the consideration of the lateral shear deformation, which is absent in lipid membranes due to lateral fluidity, is important for deriving Eq. (14). Experimental values of $\frac{\bar{k}}{k}$ lie in the range $[-1, -0.7]$ [117], leading to $\nu \in [0, 0.3]$, which contradicts volumetric incompressibility of lipid membranes, implying $\nu \approx 0.5$. Apart from Eq. (14), there are other relations between k and \bar{k} . For example, within the Helfrich Hamiltonian, the following relation holds [118,119]:

$$c_1^{\text{eq}} = c_2^{\text{eq}} = \frac{kK_0}{2k + \bar{k}}. \quad (15)$$

Here c_1^{eq} and c_2^{eq} are the principal curvatures corresponding to the local minimum of the Helfrich Hamiltonian (1). Another relation that can be obtained from the Helfrich Hamiltonian applied to constituent monolayers of a lipid bilayer is [120]

$$\bar{k}_b = 2(\bar{k}_m - 2z_0 k_m K_{0,m}), \quad (16)$$

where \bar{k}_b is the bilayer Gaussian curvature modulus. In comparison with Eqs. (15) and (16), Eq. (11) obtained in this work represents a distinct relation. Equation (11) contains only the bending modulus and the Gaussian curvature modulus, whereas Eqs. (15) and (16) contain other parameters such as K_0 in Eq. (15) and z_0 in Eq. (16). Implicitly, there is also stretching ε in Eq. (11), which enters through the derivative $\frac{d}{d\varepsilon} \bar{k}_m(\varepsilon)|_{\varepsilon=0}$. However, ε enters only locally, as the information about $\bar{k}_m(\varepsilon)$ in the vicinity of $\varepsilon = 0$ is enough to calculate the derivative of $\bar{k}_m(\varepsilon)$ with respect to ε at $\varepsilon = 0$. Because of this derivative, Eq. (11) is not of the type $\frac{\bar{k}_m}{k_m} = \text{const}$. Therefore, it should not be read from Eq. (11) that the bending modulus and Gaussian curvature modulus are not independent. Rather,

Eq. (11) shows that the bending modulus and the Gaussian curvature modulus as a function of ε , $\bar{k}_m(\varepsilon)$, are not independent. If written as

$$k_m = \frac{d}{d\varepsilon} [(1 + \varepsilon)^2 \bar{k}_m(\varepsilon)] \Big|_{\varepsilon=0}, \quad (17)$$

i.e., without expanding the brackets, Eq. (11) resembles $k_A = \frac{d}{d\varepsilon} \sigma(\varepsilon)|_{\varepsilon=0}$, the classical relation between the stretching modulus and lateral tension, and also represents the derivative of the stress-strain relation. It can be noted that, in the case of the quadratic incompressible model, it does not matter at what value of ε the derivative is taken in Eq. (17), since the bending modulus as a function of ε , $k_m(\varepsilon)$, equals $\frac{k_m}{1+\varepsilon}$, and $\frac{d}{d\varepsilon} |_{\varepsilon=\varepsilon_1} = \frac{1}{1+\varepsilon_1} \frac{d}{d\varepsilon} |_{\varepsilon=0}$ for $1 + \varepsilon = (1 + \bar{\varepsilon})(1 + \varepsilon_1)$.

D. Advantages of the proposed method

Molecular-dynamics simulations provide complete and accurate control of the state and composition of a system, which is difficult to achieve in experiments. Despite great advances in MD methods for the determination of elastic parameters of lipid membranes, there are still difficulties in their application [121]. In this section we briefly review the main approaches which are used to measure elastic parameters of lipid membranes, pointing out the advantages of the method proposed in this work compared to other MD methods.

A large and important part of MD methods is based on monitoring fluctuations [15,16,43,34,36–42] of either the membrane surface or lipid directors, i.e., the average orientations of lipid molecules. The fluctuation-based methods employ the equipartition theorem, which states that the mean energy per degree of freedom is equal to $k_B T/2$. The elastic energy of monolayer bending can be expressed either in terms of the director field \mathbf{n} as $\frac{k_m}{2} (\nabla \cdot \mathbf{n})^2$ or in terms of the intrinsic curvature and tilt \mathbf{T} as $\frac{k_m}{2} (K + \nabla \cdot \mathbf{T})^2$. From the equipartition theorem applied to the average values of the Fourier amplitudes of either the membrane surface or lipid directors, the bending modulus k_m can be determined. However, the definition of the membrane surface and lipid directors is rather ambiguous. For the definition of the membrane surface, a reference atom should be chosen, which might be either in the headgroup region or in the region of lipid tails. For the lipid director, two reference atoms should be chosen to draw a vector representing the director. The choice of these reference atoms is quite arbitrary and not strictly justified. A recent comprehensive study shows that the ambiguities in the definitions of lipid directors lead to substantial systematic errors in the values of elastic parameters [43]. For example, according to row 2 of Fig. 5 of Ref. [43], the error in the bending modulus due to the ambiguity in the definition of the lipid director can be as large as 40%. The method proposed in this work employs neither the membrane surface nor lipid directors and therefore there are no such complications with the definitions of these quantities as in fluctuation-based methods.

In the case of lipid mixtures, averaged elastic parameters are usually introduced in fluctuation-based methods. The choice of a particular averaging is questionable. For example, according to the Reuss model (12) [106], the inverse bending moduli are averaged. In a different model, the Voigt model [106], the bending moduli are averaged directly: $k_{\text{mix}} =$

$\varphi_1 k_1 + \varphi_2 k_2$, where φ_1 and φ_2 are the surface fractions of lipids of types 1 and 2, respectively. In Ref. [36], for the determination of the bending modulus of lipid mixtures from fluctuations, a model analogous to the Reuss averaging was employed. However, the validity of both the Reuss model and the Voigt model is rather vague. In this work we showed that none of these models holds for the DPPC/DOPC mixture. In the stress profiles approach, there is no need to choose an appropriate averaging, as the intrinsic bending moduli of lipid mixtures are measured directly. The same is true for the intrinsic spontaneous curvature of lipid mixtures. It should also be pointed out that the bending moduli of lipid mixtures determined by the fluctuation-based methods may correspond to not the intrinsic but the effective bending moduli due to the composition-curvature coupling [122]. Actually, the comparison of the bending modulus of lipid mixtures obtained by monitoring surface undulations with the bending modulus measured by simulating tethers showed that the former is always smaller than the latter [123], which may be due to a decrease in the bending modulus of undulating membranes because of the composition-curvature coupling effect.

There is also an open theoretical question regarding fluctuation-based methods. In particular, the theory predicts that the spectrum of $\langle |\mathbf{q} \cdot \mathbf{n}_{\mathbf{q}}|^2 \rangle$ is a decreasing function of $q \equiv |\mathbf{q}|$ [17], where \mathbf{q} is a wave vector and $\mathbf{n}_{\mathbf{q}}$ is the Fourier amplitude of lipid directors, while in simulations $\langle |\mathbf{q} \cdot \mathbf{n}_{\mathbf{q}}|^2 \rangle$ is always an increasing function [15–17,41,43]. In practice, a divergent spectrum relation is employed [15,16,43], which, however, contradicts the stability of lipid membranes, leading to unphysical results [34].

Other *in silico* methods, the equilibrium force methods, are based on applying external forces to lipid membranes and measuring the magnitude of the corresponding deformations. For example, the stretching modulus can be determined by calculating the area per lipid at different lateral tensions, i.e., forces applied to the membrane in the lateral direction [124]. The determination of the bending modulus requires a more complex procedure. One of the proposed methods [44,45] is based on membrane buckling during lateral compression: At a sufficiently high compressive force, membranes lose their initial planar state and begin to bend out of the plane. This approach requires a large lipid system to be simulated and is therefore out of reach for AA simulations. Currently, the theory for the buckling approach exists only for single-component lipid membranes [44,45]. The problem with applying the buckling approach to lipid mixtures is that in curved multicomponent membranes the lipid composition is no longer uniform due to the composition-curvature coupling effect [46,47]. Therefore, the bending energy of each monolayer in a buckled multicomponent membrane, or any curved multicomponent membrane, would be given as $\int \frac{1}{2} k_m(\mathbf{r}) [K - K_{0,m}(\mathbf{r})]^2 dS$, where the integration is over the monolayer surface, and $k_m(\mathbf{r})$ and $K_{0,m}(\mathbf{r})$ are the bending modulus and spontaneous curvature at position \mathbf{r} , respectively. Nevertheless, the theory of single-component buckled membranes can be formally employed for the determination of the bending modulus of lipid mixtures [125]. The bending modulus obtained in this formal way represents the mean bending modulus of this mixture. However, this mean value of the bending modulus is specific to the buckling procedure,

as in general $k_m(\mathbf{r})$ of membranes not bent in the same way as in the buckling procedure may be different from that of the buckled membranes and therefore the mean value of the bending modulus may also be different. The same reasoning applies to membranes curved by cylindrical repulsive walls [126]. Thus, the curvature-composition coupling represents a problem for the determination of intrinsic elastic parameters of lipid membranes using the buckling method. Also, as in the fluctuation-based methods, due to periodic boundary conditions, the buckling method does not apply to the determination of the monolayer spontaneous curvature. In the stress profile approach, lipid bilayers are always planar. Although the redistribution of lipids may nevertheless take place due to thermal undulations even in planar bilayers, on average the distribution of lipids is uniform. As the stress profile approach employs averaging over time, the local stress obtained in this way corresponds to the uniform distribution of lipids. Also, the influence of undulations on stress profiles is negligible for systems of small size (see Sec. VIE). Therefore, the stress profile protocol can be employed for the determination of intrinsic bending moduli and spontaneous curvatures.

An alternative approach for the determination of the bending modulus involves simulating tethers, or membrane tubes [127]. In this approach, a cylindrical membrane tube is created. The axial tension in these tubes is equal to $2\pi k/R$, where R is the tube radius, which allows obtaining the bending modulus k by measuring the axial tension and tube radius. The application of this method to the determination of intrinsic elastic parameters of multicomponent lipid membranes is complicated due to the difference in the curvature radii of the inner and outer monolayers of a lipid tube, which leads to the redistribution of lipids between the monolayers as a result of the composition-curvature coupling [123]. Also, the method of simulating tethers has two technical limitations related to the requirement to balance the solvent pressure outside and inside the tube, as well as to balance the area per lipid of the two monolayers [45]. By contrast, in the stress profile approach there are no such problems due to the symmetry of the flat bilayer state. Also, the method of simulating tethers does not provide values of the monolayer spontaneous curvature, unlike the method presented in this work.

Another equilibrium force method involves the analysis of a half-cylinder relaxation to a flat state [128]. Since the extrinsic curvature is not constant along the trajectory of this relaxation, this method does not apply to the calculation of intrinsic elastic parameters of lipid mixtures, as the redistribution of lipids can occur due to the composition-curvature coupling. Also, this method does not provide spontaneous curvature values. In Ref. [128] it was shown that the bending modulus depends on the extrinsic curvature. We note, however, that a thorough description of the membrane shape obtained in Ref. [128], which applies the Helfrich energy functional to each monolayer separately, restores the constancy of the bending modulus as a function of the extrinsic curvature [129].

E. Drawbacks and caveats concerning the proposed method

The method proposed in this work also has drawbacks. One of the drawbacks of the method is that the local stress is not

uniquely defined. The nonuniqueness of the local stress lies in the requirement to decompose multibody forces into pairwise forces. The cCFD that was employed in this work decomposes multibody forces into pairwise central forces between interacting particles [77]. The cCFD was introduced to overcome the difficulties of the Goetz-Lipowsky decomposition [124], which does not conserve the angular momentum of a system [77], and the central force decomposition (CFD), which is not unique for N -body potentials with $N > 4$ [77]. In Ref. [130], however, it was shown that it is possible to construct a different force decomposition for three-body potentials, the force center decomposition (FCD), by considering a force center of three interacting particles. Like the cCFD, the FCD also conserves the angular momentum of a system. Although the choice of the force decomposition does not influence the first moment of the stress profile [131], the second moment can depend on the choice of the decomposition [130]. For example, the Gaussian curvature modulus, which is equal to the second moment of the stress profile at zero stretching, of dissipative particle dynamics membranes was found to be $-3.1 \pm 0.2 k_B T$ and $-32.8 \pm 0.1 k_B T$ for the CFD and FCD, respectively [130], which is a rather large difference. In this work we used the second moment of the stress profile for the calculation of the bending modulus via Eq. (5c). Thus, although the cCFD currently represents the most natural choice for the force decomposition, the ambiguity in the definition of the local stress which is still present in the literature may lead to the ambiguity in the bending modulus obtained by the method presented in this paper. To circumvent the difficulties with the ambiguity in the definition of the local stress, a method was proposed in Refs. [131,132] that sidesteps the computation of the local stress by applying virtual bending deformations to lipid membranes and then measuring the corresponding free-energy derivatives in fluctuating planar membranes. However, in the latter approach an ambiguity remains with the choice of the center of the in-plane deformations [131].

An important limitation of the proposed method includes systems close to the phase transition. High compression of such systems can lead to phase transition. In this work, to ensure the absence of the phase transition, the compressive tensions were chosen smaller than stretching tensions: -50 and -100 bar nm for compressive tensions and $+75$ and $+150$ bar nm for stretching tensions. The maximum compression was thus 3.2%, realized in DPPC bilayers. In practice, the phase transition can be observed by a large discontinuous change in ε or stress profile data. In principle, the compression can be avoided, and the derivative with respect to stretching at $\varepsilon = 0$ can be calculated from the remaining data. However, this would require more data at positive tension to stay within the same error limits.

In real systems and simulations, lipid membranes undergo fluctuations due to thermal motion, resulting in out-of-plane undulations. The excess area, absorbed by these undulations, may lead to corrections to the observed values of forces and apparent stretching [100,121,133]. This is especially important for large systems since the contribution of the excess area is also large. However, for small systems the corrections are minor. For example, for systems approximately equal to

$45 \times 7 \text{ nm}^2$ in size used in the buckling method, the corrections do not exceed 1% [45]. In our case, the considered systems are even smaller, with the lateral size of the box being approximately equal to 10 nm. Therefore, we did not include the effect of thermal fluctuations in the analysis of the elastic parameters.

Simulations with too small a system size can also be problematic due to the periodic boundary conditions since for too small a simulation box the configurations of lipid molecules can be correlated with their periodic images. To estimate the smallest box size, beyond which these correlations become important, let us consider the characteristic length l of lipid monolayer deformations. According to Ref. [134], $l = h_m^2 \sqrt{\frac{k_t}{k_m}}$, where h_m , k_m , and k_t are the monolayer hydrophobic thickness, bending modulus, and tilt modulus, respectively. The typical values of h_m , k_m , and k_t are 1.5 nm [35], $12 k_B T$ [100], and $12 k_B T \text{ nm}^{-2}$ [100], respectively, implying $l \approx 2.25$ nm. Thus, the smallest side length of the simulation box can be estimated as $L_{\min} = 2l = 4.5$ nm. Since the typical area per lipid is approximately equal to $a_l = 0.6 \text{ nm}^2$ [135], the minimum number of lipids per leaflet can be estimated as $L_{\min}^2/a_l \approx 34$. A similar number of lipids, 36 per leaflet, is frequently employed in MD simulations of lipid bilayers [38,105].

In this work CG models were used; however, the proposed method applies to any lipid system which allows the calculation of the stress profile, including AA ones. The CG models were chosen not only due to their speed but also because the current version of GROMACS-LS does include the particle-mesh Ewald method for the electrostatic calculation needed for AA simulations, without which the calculation is computationally expensive [75]. We note that going from CG to AA systems would not necessarily involve using the same $1\text{-}\mu\text{s}$ simulation time per tension as was used in this work, which is quite a long time for AA simulations. All-atom systems have a higher number of interacting particles and therefore more statistics compared to CG systems. For example, simulating 72 AA DPPC lipids for 139 ns at 323 K leads to the same error of $0.03 k_B T \text{ nm}^{-1}$ for the first moment of the stress profile [105] as that obtained in this work for 256 CG DPPC lipids simulated for $1 \mu\text{s}$. To obtain the exact scaling function, additional simulations at different isotropic ambient pressures are required, which may lead to the overall simulation time of 1390 ns, if five different tensions and isotropic ambient pressures are considered as in this work. Nevertheless, the overall complexity in terms of ns \times lipid is not much larger than that of, for example, fluctuation-based methods. The smallest system reported in the fluctuation-based approaches was 288 AA DPPC simulated for 200 ns at 323 K [42], which resulted in the same error of $0.6 k_B T$ for the monolayer bending modulus as in this work. The complexity of 288 AA DPPC simulated for 200 ns is $200 \text{ ns} \times 288 \text{ lipids} = 57\,600 \text{ ns} \times \text{lipid}$, which is approximately 1.7 times less complex than $1390 \text{ ns} \times 72 \text{ lipids} = 100\,080 \text{ ns} \times \text{lipid}$. However, one should also take into account the time required to obtain stress profiles, which in our case was about 1/3 of the simulation time.

VII. CONCLUSION

In this work, within the framework of the classical 3D theory of elasticity, we considered the stress-strain relation of planar lipid bilayers. We revised the theory of Campelo *et al.* [31] and developed the method for the determination of the following monolayer elastic parameters of lipid membranes: bending and stretching moduli, spontaneous curvature, neutral surface position, and local Poisson's ratio. An important correction to the expression for the local stretching modulus was found [Eq. (12)], which if not taken into account can lead to large systematic errors up to $24 \pm 5\%$ for the bending moduli. Unlike previous considerations, we assumed a more general condition of global incompressibility instead of local incompressibility. This allowed us to derive the expression (9) for the local Poisson's ratio of lipid membranes $\nu(z)$, which can be determined through the response of the local lateral stress profile to the change of the isotropic ambient pressure. Using $\nu(z)$, we determined the exact scaling map, i.e., a function that determines how the thickness of lipid monolayers changes locally upon stretching or compression, necessary for finding the correspondence between the points of the stress profiles obtained at different lateral tensions. By introducing the local tension profile at different stretching, we showed that the approach of Campelo *et al.* for the determination of elastic parameters can be largely simplified: Elastic parameters can be determined with one quadratic fit of tension profile moments obtained at different stretching according to Eqs. (5a)–(5c) instead of first calculating the local stretching modulus and then using Eqs. (4a)–(4c). In the case of a simplified assumption of the local incompressibility and quadratic energy law, a relation was found between the bending modulus and Gaussian curvature modulus as a function of stretching [Eq. (11)], which shows that these two moduli are not completely independent, as was previously assumed. The theoretical results were applied to the CG MD simulations of DPPC, DOPC, and their 50:50 mixture. The following elastic parameters were determined: the stretching and bending moduli, neutral surface position, spontaneous curvature, and local Poisson's ratio. The local Poisson's ratio was determined from the local stress. The bending modulus and spontaneous curvature of the DPPC/DOPC mixture were interpreted as intrinsic parameters corresponding to no composition-curvature coupling. It was shown that the dependence of the intrinsic bending modulus of the DPPC/DOPC mixture is more complex than predicted by the classical Reuss averaging, which is often used in theoretical frameworks.

ACKNOWLEDGMENT

The work was supported by the Russian Science Foundation Grant No. 22-24-00661.

APPENDIX A: VARIATION OF THE ELASTIC ENERGY

In this appendix we derive the expression for the local tension, Eq. (6). The elastic energy function of the monolayer is given by $W(\varepsilon, z)$. To perform the variation with respect to ε , we need to provide the geometrical structure that this energy function describes. To do this, we follow the approach

suggested in Ref. [136], wherein the geometry is specified using Lagrange multipliers. Let us first introduce the coordinate system (x_1, x_2, x_3) , the x_3 axis of which is directed along the lipid tails from the hydrophilic to the hydrophobic part of the monolayer, and x_1 and x_2 describe the points of the transverse planes at a given value of x_3 . Using this coordinate system, we can describe the points of the initial and deformed states of the monolayer using the vector functions $\mathbf{R}_0(x_1, x_2, x_3)$ and $\mathbf{R}(x_1, x_2, x_3)$, respectively. These functions define local bases and metric tensors via $\mathbf{e}_{0a} \equiv \partial_a \mathbf{R}_0$, $\mathbf{e}_a \equiv \partial_a \mathbf{R}$, $g_{0ab} \equiv \mathbf{e}_{0a} \cdot \mathbf{e}_{0b}$, $g_{ab} \equiv \mathbf{e}_a \cdot \mathbf{e}_b$, $g_0 \equiv \det g_{0ab}$, $g \equiv \det g_{ab}$ ($a, b = 1, 2, 3$), and the area densities of the transverse planes x_1 and x_2 : $\hat{g} = \det g_{ab}$ and $\hat{g}_0 = \det g_{0ab}$ ($a, b = 1, 2$). Now we can construct the Hamiltonian

$$\begin{aligned} H = & \int W(\varepsilon) dV_0 \\ & + \int [\mathbf{f}^a (\mathbf{e}_a - \nabla_a \mathbf{R}) + \mathbf{f}_0^a (\mathbf{e}_{0a} - \nabla_a \mathbf{R}_0)] dV \\ & + \int [\lambda^{ab} (g_{ab} - \mathbf{e}_a \cdot \mathbf{e}_b) + \lambda_0^{ab} (g_{0ab} - \mathbf{e}_{0a} \cdot \mathbf{e}_{0b})] dV \\ & + \int \left[P \left(\frac{\sqrt{g}}{\sqrt{g_0}} - \beta(\varepsilon) \right) \right] dV \\ & + \int \left[\lambda_\varepsilon \left(\frac{\sqrt{\hat{g}}}{\sqrt{\hat{g}_0}} - (1 + \varepsilon) \right) \right] dV, \end{aligned} \quad (\text{A1})$$

where $a, b = 1, 2, 3$ and the summation over repeated indices (one upper and one lower) is implied; $dV_0 = \sqrt{g_0} dx_1 dx_2 dx_3$; $dV = \sqrt{g} dx_1 dx_2 dx_3$; and H is a function of ε , \mathbf{e}_a , \mathbf{e}_{0a} , \mathbf{R} , \mathbf{R}_0 , g_{ab} , and g_{0ab} , the definitions of which are captured by the Lagrange multipliers \mathbf{f}^a , \mathbf{f}_0^a , λ^{ab} , λ_0^{ab} , P , and λ_ε . For brevity, the explicit dependence of β and W on x_3 was omitted. The Lagrange multiplier \mathbf{f}^a corresponds to the stress tensor Σ via the relation $\Sigma = -\mathbf{f}^a \otimes \mathbf{e}_a$, where \otimes is the outer product [117,137]. To find \mathbf{f}^a , we perform the variation of H with respect to ε , \mathbf{e}_a , \mathbf{e}_{0a} , g_{ab} , and g_{0ab} and obtain the system of equations

$$\begin{aligned} -P\beta(\varepsilon) \frac{\partial \beta(\varepsilon)}{\partial \varepsilon} - \beta(\varepsilon)\lambda_\varepsilon + \frac{\partial W(\varepsilon)}{\partial \varepsilon} &= 0 \quad \text{for } \varepsilon, \\ -2\lambda_0^{ab} \mathbf{e}_{0b} + \mathbf{f}_0^a &= 0 \quad (a, b = 1, 2, 3) \quad \text{for } \mathbf{e}_{0a}, \\ -2\lambda^{ab} \mathbf{e}_b + \mathbf{f}^a &= 0 \quad (a, b = 1, 2, 3) \quad \text{for } \mathbf{e}_a, \\ [-\beta(\varepsilon)^2 P + W(\varepsilon)] g^{03a} & \\ + 2\lambda_0^{3a} \beta(\varepsilon) &= 0 \quad (a = 1, 2, 3) \quad \text{for } g_{03a}, \\ -\beta(\varepsilon)\lambda_\varepsilon(1 + \varepsilon) g^{0ab} + [-\beta(\varepsilon)^2 P + W(\varepsilon)] g^{0ab} & \\ + 2\lambda_0^{ab} \beta(\varepsilon) &= 0 \quad (a, b = 1, 2) \quad \text{for } g_{0ab}, \\ P\beta(\varepsilon) g^{3a} + 2\lambda^{3a} &= 0 \quad (a = 1, 2, 3) \quad \text{for } g_{3a}, \\ \lambda_\varepsilon(1 + \varepsilon) g^{ab} + P\beta(\varepsilon) g^{ab} & \\ + 2\lambda^{ab} &= 0 \quad (a, b = 1, 2) \quad \text{for } g_{ab}, \end{aligned} \quad (\text{A2})$$

where each equation corresponds to the variation with respect to the variable written on the right. To perform the variation with respect to the components of the metric tensors, we used the relations $\partial g / \partial g_{ab} = g g^{ab}$ and $\partial g_0 / \partial g_{0ab} = g_0 g_0^{ab}$ for $a, b = 1, 2, 3$ and $\partial \hat{g} / \partial g_{ab} = \hat{g} g^{ab}$ and $\partial \hat{g}_0 / \partial g_{0ab} = \hat{g}_0 g_0^{ab}$ for $a, b = 1, 2$. We omitted λ^{a3} due to the symmetry of λ^{ab} ,

$a, b = 1, 2, 3$. Note that, in general, $\partial \hat{g} / \partial g_{ab} \neq \hat{g}^{ab}$, but in our case $\partial \mathbf{R} / \partial x_3$ is always perpendicular to $\partial \mathbf{R} / \partial x_a$, $a = 1, 2$, as we do not consider tilt deformations. From Eqs. (A2) we see that the variations with respect to the variables with index 0 are decoupled from the rest.

The system of equations (A2) can be solved step by step as

$$\begin{aligned} \lambda_\varepsilon &= \frac{\frac{\partial W(\varepsilon)}{\partial \varepsilon} - P\beta(\varepsilon)\frac{\partial \beta(\varepsilon)}{\partial \varepsilon}}{\beta(\varepsilon)}, \\ \lambda^{ab} &= \frac{g^{ab}\left(-\frac{\partial W(\varepsilon)}{\partial \varepsilon}(1+\varepsilon) - P\beta(\varepsilon)^2 + P\beta(\varepsilon)(1+\varepsilon)\frac{\partial \beta(\varepsilon)}{\partial \varepsilon}\right)}{2\beta(\varepsilon)}, \\ \lambda^{3a} &= -\frac{P\beta(\varepsilon)g^{3a}}{2}, \quad a = 1, 2, 3, \\ \mathbf{f}^a &= \frac{-\frac{\partial W(\varepsilon)}{\partial \varepsilon}(1+\varepsilon) - P\beta(\varepsilon)^2 + P\beta(\varepsilon)(1+\varepsilon)\frac{\partial \beta(\varepsilon)}{\partial \varepsilon}}{\beta(\varepsilon)}\mathbf{e}^a, \\ \mathbf{f}^3 &= -P\beta(\varepsilon)\mathbf{e}^3, \end{aligned} \quad (\text{A3})$$

where $\mathbf{e}^a \equiv g^{ab}\mathbf{e}_b$, with $a, b = 1, 2, 3$. Recall that, for brevity, we have so far omitted the explicit dependence of W and β on x_3 . Now, choosing the previously introduced z axis as the x_3 axis, we can construct the local stress tensor

$$\begin{aligned} \Sigma(\varepsilon, z) &\equiv -\mathbf{f}^a \otimes \mathbf{e}_a \\ &= \frac{\frac{\partial W(\varepsilon, z)}{\partial \varepsilon}(1+\varepsilon) + P\beta(\varepsilon, z)^2 - P\beta(\varepsilon, z)(1+\varepsilon)\frac{\partial \beta}{\partial \varepsilon}(\varepsilon, z)}{\beta(\varepsilon, z)} \\ &\quad \times (\mathbf{1} - \mathbf{N} \otimes \mathbf{N}) + P\beta(\varepsilon, z)\mathbf{N} \otimes \mathbf{N}, \end{aligned} \quad (\text{A4})$$

where $\mathbf{1}$ is the unit matrix and \mathbf{N} the unit normal along the z axis. The Σ acts in the following way: An outward unit normal to some region gives the force per unit area onto this region. The terms multiplying $\mathbf{1} - \mathbf{N} \otimes \mathbf{N}$ and $\mathbf{N} \otimes \mathbf{N}$ in Eq. (A4) correspond to the lateral and normal parts of the stress tensor. In equilibrium, the normal force is constant, i.e., $P\beta(\varepsilon, z) = \text{const} = -P_z$, where P_z is the value of the normal pressure. Inserting $P\beta(\varepsilon, z) = -P_z$ into Eq. (A4), we obtain

$$\begin{aligned} \Sigma(\varepsilon, z) &\equiv -\mathbf{f}^a \otimes \mathbf{e}_a \\ &= \frac{\frac{\partial W(\varepsilon, z)}{\partial \varepsilon}(1+\varepsilon) - P_z\beta(\varepsilon, z) + P_z(1+\varepsilon)\frac{\partial \beta}{\partial \varepsilon}(\varepsilon, z)}{\beta(\varepsilon, z)} \\ &\quad \times (\mathbf{1} - \mathbf{N} \otimes \mathbf{N}) - P_z\mathbf{N} \otimes \mathbf{N}. \end{aligned} \quad (\text{A5})$$

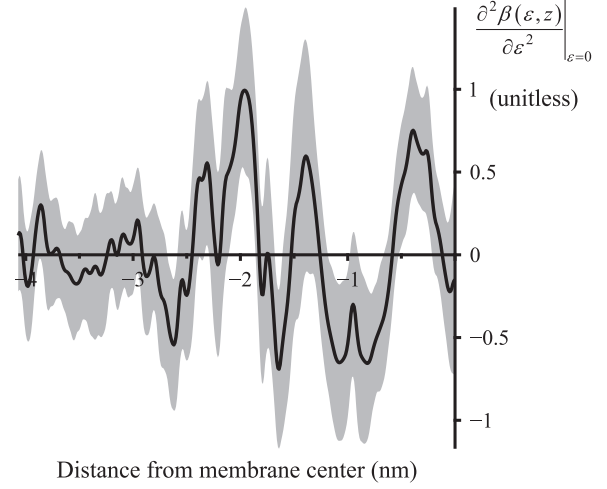


FIG. 5. Plot of $\frac{\partial^2 \beta(\varepsilon, z)}{\partial \varepsilon^2} \Big|_{\varepsilon=0}$ as a function of the distance from the membrane center. The black curve and gray shading are the mean value and 95% confidence band, respectively.

The local tension is by definition equal to $\frac{\partial W(\varepsilon, z)}{\partial \varepsilon}$ and we can express it from Σ as

$$\sigma(\varepsilon, z) \equiv \frac{\partial W(\varepsilon, z)}{\partial \varepsilon} = \frac{[S(\varepsilon, z, P_z) + P_z]\beta(\varepsilon, z)}{1+\varepsilon} - P_z \frac{\partial \beta(\varepsilon, z)}{\partial \varepsilon}, \quad (\text{A6})$$

where $S(\varepsilon, z, P_z)$ is the lateral stress, i.e., the lateral part of Σ .

APPENDIX B: SECOND DERIVATIVE OF $\beta(\varepsilon, z)$

In this appendix we provide an expression and a measured value for $\frac{\partial^2 \beta(\varepsilon, z)}{\partial \varepsilon^2} \Big|_{\varepsilon=0}$. Taking the derivative of Eq. (6) with respect to P_z and then with respect to ε , we find

$$\frac{\partial^2 \beta(\varepsilon, z)}{\partial \varepsilon^2} \Big|_{\varepsilon=0} = \frac{\partial}{\partial \varepsilon} \left[\left(\frac{\partial S(\varepsilon, z, P_z)}{\partial P_z} + 1 \right) \frac{\beta(\varepsilon, z)}{1+\varepsilon} \right] \Big|_{\varepsilon=0}. \quad (\text{B1})$$

To find $\frac{\partial S(\varepsilon, z, P_z)}{\partial P_z}$, at a given fixed tension, corresponding to stretching ε , we varied P_z , setting the values of P_z to $-50, -25, 1, 25,$ and 50 bar. The scaling function and $\beta(\varepsilon, z)$ on the right-hand side of Eq. (B1) were approximated by the linear relation $\beta(\varepsilon, z) = 1 + \gamma(z)\varepsilon$. The resulting values of $\frac{\partial^2 \beta(\varepsilon, z)}{\partial \varepsilon^2} \Big|_{\varepsilon=0}$ are shown in Fig. 5.

From Fig. 5 it follows that the maximum absolute value of $\frac{\partial^2 \beta(\varepsilon, z)}{\partial \varepsilon^2} \Big|_{\varepsilon=0}$ does not exceed approximately 1.5. The moments $P_z \int_{m_0} \frac{\partial^2 \beta(\varepsilon, z)}{\partial \varepsilon^2} \Big|_{\varepsilon=0} (z - z_0)^n dz$ relative to the location of the neutral surface, $z_0 \approx -1.2$, at $P_z = 1$ bar, are $0.002 \pm 0.002 k_B T \text{ nm}^{-2}$, $-0.0006 \pm 0.0037 k_B T \text{ nm}^{-1}$, and $0.002 \pm 0.007 k_B T$ for $n = 0, 1,$ and 2 , respectively, and thus are negligibly small in comparison with the elastic parameters of DPPC.

[1] L. D. Nelson and M. M. Cox, *Lehninger Principles of Biochemistry* (Freeman, New York, 2004).

[2] P. I. Kuzmin, J. Zimmerberg, Y. A. Chizmadzhev, and F. S. Cohen, A quantitative model for membrane fusion based on

- low-energy intermediates, *Proc. Natl. Acad. Sci. USA* **98**, 7235 (2001).
- [3] P. V. Bashkirov, S. A. Akimov, A. I. Evseev, S. L. Schmid, J. Zimmerberg, and V. A. Frolov, GTPase cycle of dynamin is coupled to membrane squeeze and release, leading to spontaneous fission, *Cell* **135**, 1276 (2008).
- [4] K. V. Pinigin, O. V. Kondrashov, I. Jiménez-Munguía, V. V. Alexandrova, O. V. Batishchev, T. R. Galimzyanov, and S. A. Akimov, Elastic deformations mediate interaction of the raft boundary with membrane inclusions leading to their effective lateral sorting, *Sci. Rep.* **10**, 4087 (2020).
- [5] A. V. Shnyrova, P. V. Bashkirov, S. A. Akimov, T. J. Pucadyil, J. Zimmerberg, S. L. Schmid, and V. A. Frolov, Geometric catalysis of membrane fission driven by flexible dynamin rings, *Science* **339**, 1433 (2013).
- [6] Y. Kozlovsky and M. M. Kozlov, Stalk model of membrane fusion: Solution of energy crisis, *Biophys. J.* **82**, 882 (2002).
- [7] V. S. Markin and J. P. Albanesi, Membrane fusion: Stalk model revisited, *Biophys. J.* **82**, 693 (2002).
- [8] R. L. Knorr, R. Dimova, and R. Lipowsky, Curvature of double-membrane organelles generated by changes in membrane size and composition, *PLoS One* **7**, e32753 (2012).
- [9] S. A. Akimov, P. E. Volynsky, T. R. Galimzyanov, P. I. Kuzmin, K. V. Pavlov, and O. V. Batishchev, Pore formation in lipid membrane I: Continuous reversible trajectory from intact bilayer through hydrophobic defect to transversal pore, *Sci. Rep.* **7**, 12509 (2017).
- [10] S. A. Akimov, P. E. Volynsky, T. R. Galimzyanov, P. I. Kuzmin, K. V. Pavlov, and O. V. Batishchev, Pore formation in lipid membrane II: Energy landscape under external stress, *Sci. Rep.* **7**, 12152 (2017).
- [11] J. B. Fournier, Microscopic membrane elasticity and interactions among membrane inclusions: Interplay between the shape, dilation, tilt and tilt-difference modes, *Eur. Phys. J. B* **11**, 261 (1999).
- [12] S. May and A. Ben-Shaul, Molecular theory of lipid-protein interaction and the L_{α} -HII transition, *Biophys. J.* **76**, 751 (1999).
- [13] W. Helfrich, Elastic properties of lipid bilayers: Theory and possible experiments, *Z. Naturforsch. C* **28**, 693 (1973).
- [14] M. Hamm and M. M. Kozlov, Elastic energy of tilt and bending of fluid membranes, *Eur. Phys. J. E* **3**, 323 (2000).
- [15] M. M. Terzi and M. Deserno, Novel tilt-curvature coupling in lipid membranes, *J. Chem. Phys.* **147**, 084702 (2017).
- [16] M. M. Terzi, M. F. Ergüder, and M. Deserno, A consistent quadratic curvature-tilt theory for fluid lipid membranes, *J. Chem. Phys.* **151**, 164108 (2019).
- [17] K. V. Pinigin, P. I. Kuzmin, S. A. Akimov, and T. R. Galimzyanov, Additional contributions to elastic energy of lipid membranes: Tilt-curvature coupling and curvature gradient, *Phys. Rev. E* **102**, 042406 (2020).
- [18] V. A. Frolov, A. Escalada, S. A. Akimov, and A. V. Shnyrova, Geometry of membrane fission, *Chem. Phys. Lipids* **185**, 129 (2015).
- [19] S. Marčelja, Lipid-mediated protein interaction in membranes, *Biochim. Biophys. Acta* **455**, 1 (1976).
- [20] P. Lagüe, M. J. Zuckermann, and B. Roux, Lipid-mediated interactions between intrinsic membrane proteins: Dependence on protein size and lipid composition, *Biophys. J.* **81**, 276 (2001).
- [21] K. Bohinc, V. Kralj-Iglič, and S. May, Interaction between two cylindrical inclusions in a symmetric lipid bilayer, *J. Chem. Phys.* **119**, 7435 (2003).
- [22] M. M. Müller, M. Deserno, and J. Guven, Interface-mediated interactions between particles: A geometrical approach, *Phys. Rev. E* **72**, 061407 (2005).
- [23] K. V. Pinigin, M. V. Volovik, O. V. Batishchev, and S. A. Akimov, Interaction of ordered lipid domain boundaries and amphipathic peptides regulates probability of pore formation in membranes, *Biol. Membr.* **14**, 319 (2020).
- [24] K. V. Pinigin, T. R. Galimzyanov, and S. A. Akimov, Interaction of ordered lipid domains in the presence of amphipathic peptides, *Biol. Membr.* **15**, 219 (2021).
- [25] K. V. Pinigin, T. R. Galimzyanov, and S. A. Akimov, Amphipathic peptides impede lipid domain fusion in phase-separated membranes, *Membranes* **11**, 797 (2021).
- [26] T. R. Galimzyanov, R. J. Molotkovsky, M. E. Bozdaganyan, F. S. Cohen, P. Pohl, and S. A. Akimov, Elastic Membrane Deformations Govern Interleaflet Coupling of Lipid-Ordered Domains, *Phys. Rev. Lett.* **115**, 088101 (2015).
- [27] F. Campelo, H. T. McMahon, and M. M. Kozlov, The hydrophobic insertion mechanism of membrane curvature generation by proteins, *Biophys. J.* **95**, 2325 (2008).
- [28] A. J. Sodt and R. W. Pastor, Molecular modeling of lipid membrane curvature induction by a peptide: More than simply shape, *Biophys. J.* **106**, 1958 (2014).
- [29] A. J. Sodt, A. H. Beaven, O. S. Andersen, W. Im, and R. W. Pastor, Gramicidin a channel formation induces local lipid redistribution II: A 3D continuum elastic model, *Biophys. J.* **112**, 1198 (2017).
- [30] W. Helfrich, Blocked lipid exchange in bilayers and its possible influence on the shape of vesicles, *Z. Naturforsch. C* **29**, 510 (1974).
- [31] F. Campelo, C. Arnarez, S. J. Marrink, and M. M. Kozlov, Helfrich model of membrane bending: From Gibbs theory of liquid interfaces to membranes as thick anisotropic elastic layers, *Adv. Colloid Interface Sci.* **208**, 25 (2014).
- [32] S. J. Marrink, H. J. Risselada, S. Yefimov, D. P. Tieleman, and A. H. De Vries, The MARTINI force field: Coarse grained model for biomolecular simulations, *J. Phys. Chem. B* **111**, 7812 (2007).
- [33] B. Różycki and R. Lipowsky, Spontaneous curvature of bilayer membranes from molecular simulations: Asymmetric lipid densities and asymmetric adsorption, *J. Chem. Phys.* **142**, 054101 (2015).
- [34] M. C. Watson, E. S. Penev, P. M. Welch, and F. L. Brown, Thermal fluctuations in shape, thickness, and molecular orientation in lipid bilayers, *J. Chem. Phys.* **135**, 244701 (2011).
- [35] R. M. Venable, F. L. Brown, and R. W. Pastor, Mechanical properties of lipid bilayers from molecular dynamics simulation, *Chem. Phys. Lipids* **192**, 60 (2015).
- [36] G. Khelashvili, B. Kollmitzer, P. Heftberger, G. Pabst, and D. Harries, Calculating the bending modulus for multicomponent lipid membranes in different thermodynamic phases, *J. Chem. Theory Comput.* **9**, 3866 (2013).

- [37] R. Goetz, G. Gompper, and R. Lipowsky, Mobility and Elasticity of Self-Assembled Membranes, *Phys. Rev. Lett.* **82**, 221 (1999).
- [38] S. E. Feller and R. W. Pastor, Constant surface tension simulations of lipid bilayers: The sensitivity of surface areas and compressibilities, *J. Chem. Phys.* **111**, 1281 (1999).
- [39] E. Lindahl and O. Edholm, Mesoscopic undulations and thickness fluctuations in lipid bilayers from molecular dynamics simulations, *Biophys. J.* **79**, 426 (2000).
- [40] E. R. May, A. Narang, and D. I. Kopelevich, Role of molecular tilt in thermal fluctuations of lipid membranes, *Phys. Rev. E* **76**, 021913 (2007).
- [41] M. C. Watson, E. G. Brandt, P. M. Welch, and F. L. Brown, Determining Biomembrane Bending Rigidities from Simulations of Modest Size, *Phys. Rev. Lett.* **109**, 028102 (2012).
- [42] Z. A. Levine, R. M. Venable, M. C. Watson, M. G. Lerner, J. E. Shea, R. W. Pastor, and F. L. Brown, Determination of biomembrane bending moduli in fully atomistic simulations, *J. Am. Chem. Soc.* **136**, 13582 (2014).
- [43] M. F. Ergüder and M. Deserno, Identifying systematic errors in a power spectral analysis of simulated lipid membranes, *J. Chem. Phys.* **154**, 214103 (2021).
- [44] H. Noguchi, Anisotropic surface tension of buckled fluid membranes, *Phys. Rev. E* **83**, 061919 (2011).
- [45] M. Hu, P. Diggins, IV, and M. Deserno, Determining the bending modulus of a lipid membrane by simulating buckling, *J. Chem. Phys.* **138**, 214110 (2013).
- [46] T. Baumgart, B. R. Capraro, C. Zhu, and S. L. Das, Thermodynamics and mechanics of membrane curvature generation and sensing by proteins and lipids, *Annu. Rev. Phys. Chem.* **62**, 483 (2011).
- [47] P. V. Bashkirov, P. I. Kuzmin, J. V. Lillo, and V. A. Frolov, Molecular shape solution for mesoscopic remodeling of cellular membranes, *Annu. Rev. Biophys.* **51**, 473 (2022).
- [48] L. F. Braganza and D. L. Worcester, Structural changes in lipid bilayers and biological membranes caused by hydrostatic pressure, *Biochemistry* **25**, 7484 (1986).
- [49] S. F. Scarlata, Compression of lipid membranes as observed at varying membrane positions, *Biophys. J.* **60**, 334 (1991).
- [50] R. E. Tosh and P. J. Collings, High pressure volumetric measurements in dipalmitoylphosphatidylcholine bilayers, *Biochim. Biophys. Acta* **859**, 10 (1986).
- [51] N. Vennemann, M. D. Lechner, T. Henkel, and W. Knoll, Densitometric characterization of the main phase transition of dimyristoyl-phosphatidylcholine between 0.1 and 40 MPa, *Ber. Bunsenges. Phys. Chem.* **90**, 888 (1986).
- [52] M. M. Terzi, M. Deserno, and J. F. Nagle, Mechanical properties of lipid bilayers: A note on the Poisson ratio, *Soft Matter* **15**, 9085 (2019).
- [53] A. Tardieu, V. Luzzati, and F. C. Reman, Structure and polymorphism of the hydrocarbon chains of lipids: A study of lecithin-water phases, *J. Mol. Biol.* **75**, 711 (1973).
- [54] G. Van Meer, D. R. Voelker, and G. W. Feigenson, Membrane lipids: Where they are and how they behave, *Nat. Rev. Mol. Cell Biol.* **9**, 112 (2008).
- [55] U. Bernchou, J. Brewer, H. S. Midtby, J. H. Ipsen, L. A. Bagatolli, and A. C. Simonsen, Texture of lipid bilayer domains, *J. Am. Chem. Soc.* **131**, 14130 (2009).
- [56] A. B. Cairns and A. L. Goodwin, Negative linear compressibility, *Phys. Chem. Chem. Phys.* **17**, 20449 (2015).
- [57] O. Berger, O. Edholm, and F. Jähnig, Molecular dynamics simulations of a fluid bilayer of dipalmitoylphosphatidylcholine at full hydration, constant pressure, and constant temperature, *Biophys. J.* **72**, 2002 (1997).
- [58] R. M. Venable, A. Skibinsky, and R. W. Pastor, Constant surface tension molecular dynamics simulations of lipid bilayers with trehalose, *Mol. Simul.* **32**, 849 (2006).
- [59] R. A. Fine and F. J. Millero, Compressibility of water as a function of temperature and pressure, *J. Chem. Phys.* **59**, 5529 (1973).
- [60] W. Rawicz, K. C. Olbrich, T. McIntosh, D. Needham, and E. A. Evans, Effect of chain length and unsaturation on elasticity of lipid bilayers, *Biophys. J.* **79**, 328 (2000).
- [61] L. D. Landau and E. M. Lifshitz, *Course of Theoretical Physics* (Pergamon, Oxford, 1975), Vol. 7.
- [62] V. S. Markin, M. M. Kozlov, and S. L. Leikin, Definition of surface tension at a non-spherical interface, *J. Chem. Soc. Faraday Trans. 2* **84**, 1149 (1988).
- [63] W. Helfrich, Lyotropic lamellar phases, *J. Phys.: Condens. Matter* **6**, A79 (1994).
- [64] I. Szleifer, D. Kramer, A. Ben-Shaul, W. M. Gelbart, and S. A. Safran, Molecular theory of curvature elasticity in surfactant films, *J. Chem. Phys.* **92**, 6800 (1990).
- [65] P. C. Souza, R. Alessandri, J. Barnoud, S. Thallmair, I. Faustino, F. Grünewald, I. Patmanidis, H. Abdizadeh, B. M. Bruininks, A. T. Wassenaar *et al.*, Martini 3: A general purpose force field for coarse-grained molecular dynamics, *Nat. Methods* **18**, 382 (2021).
- [66] M. J. Ruocco and G. G. Shipley, Characterization of the sub-transition of hydrated dipalmitoylphosphatidylcholine bilayers. Kinetic, hydration and structural study, *Biochim. Biophys. Acta* **691**, 309 (1982).
- [67] K. Åman, E. Lindahl, O. Edholm, P. Håkansson, and P. O. Westlund, Structure and dynamics of interfacial water in an L_{α} phase lipid bilayer from molecular dynamics simulations, *Biophys. J.* **84**, 102 (2003).
- [68] M. J. Abraham, T. Murtola, R. Schulz, S. Páll, J. C. Smith, B. Hess, and E. Lindahl, GROMACS: High performance molecular simulations through multi-level parallelism from laptops to supercomputers, *SoftwareX* **1**, 19 (2015).
- [69] D. Van Der Spoel, E. Lindahl, B. Hess, G. Groenhof, A. E. Mark, and H. J. Berendsen, GROMACS: Fast, flexible, and free, *J. Comput. Chem.* **26**, 1701 (2005).
- [70] G. Bussi, D. Donadio, and M. Parrinello, Canonical sampling through velocity rescaling, *J. Chem. Phys.* **126**, 014101 (2007).
- [71] H. J. C. Berendsen, J. P. M. Postma, W. F. van Gunsteren, A. DiNola, and J. R. Haak, Molecular dynamics with coupling to an external bath, *J. Chem. Phys.* **81**, 3684 (1984).
- [72] S. Jo, T. Kim, and W. Im, Automated builder and database of protein/membrane complexes for molecular dynamics simulations, *PLoS One* **2**, e880 (2007).
- [73] S. Jo, J. B. Lim, J. B. Klauda, and W. Im, CHARMM-GUI membrane builder for mixed bilayers and its application to yeast membranes, *Biophys. J.* **97**, 50 (2009).
- [74] S. Jo, T. Kim, V. G. Iyer, and W. Im, CHARMM-GUI: A web-based graphical user interface for CHARMM, *J. Comput. Chem.* **29**, 1859 (2008).

- [75] J. M. Vanegas, A. Torres-Sánchez, and M. Arroyo, Importance of force decomposition for local stress calculations in biomembrane molecular simulations, *J. Chem. Theory Comput.* **10**, 691 (2014).
- [76] A. Torres-Sánchez, J. M. Vanegas, and M. Arroyo, Examining the Mechanical Equilibrium of Microscopic Stresses in Molecular Simulations, *Phys. Rev. Lett.* **114**, 258102 (2015).
- [77] A. Torres-Sánchez, J. M. Vanegas, and M. Arroyo, Geometric derivation of the microscopic stress: A covariant central force decomposition, *J. Mech. Phys. Solids* **93**, 224 (2016).
- [78] O. S. Ollila, H. J. Risselada, M. Louhivuori, E. Lindahl, I. Vattulainen, and S. J. Marrink, 3D Pressure Field in Lipid Membranes and Membrane-Protein Complexes, *Phys. Rev. Lett.* **102**, 078101 (2009).
- [79] A. Hossein and M. Deserno, Stiffening transition in asymmetric lipid bilayers: The role of highly ordered domains and the effect of temperature and size, *J. Chem. Phys.* **154**, 014704 (2021).
- [80] D. J. Steigmann, A model for lipid membranes with tilt and distension based on three-dimensional liquid crystal theory, *Int. J. Non-Linear Mech.* **56**, 61 (2013).
- [81] J. Árnadóttir and M. Chalfie, Eukaryotic mechanosensitive channels, *Annu. Rev. Biophys.* **39**, 111 (2010).
- [82] E. S. Haswell, R. Phillips, and D. C. Rees, Mechanosensitive channels: What can they do and how do they do it? *Structure* **19**, 1356 (2011).
- [83] E. Falck, M. Patra, M. Karttunen, M. T. Hyvönen, and I. Vattulainen, Lessons of slicing membranes: Interplay of packing, free area, and lateral diffusion in phospholipid/cholesterol bilayers, *Biophys. J.* **87**, 1076 (2004).
- [84] M. Kupiainen, E. Falck, S. Ollila, P. Niemelä, A. A. Gurtovenko, M. T. Hyvönen, M. Patra, M. Karttunen, and I. Vattulainen, Free volume properties of sphingomyelin, DMPC, DPPC, and PLPC bilayers, *J. Comput. Theor. Nanosci.* **2**, 401 (2005).
- [85] J. B. Fournier, Coupling between membrane tilt-difference and dilation: A new “ripple” instability and multiple crystalline inclusions phases, *Europhys. Lett.* **43**, 725 (1998).
- [86] S. May, Y. Kozlovsky, A. Ben-Shaul, and M. M. Kozlov, Tilt modulus of a lipid monolayer, *Eur. Phys. J. E* **14**, 299 (2004).
- [87] M. Fošnarčič, A. Iglič, and S. May, Influence of rigid inclusions on the bending elasticity of a lipid membrane, *Phys. Rev. E* **74**, 051503 (2006).
- [88] D. I. Kopelevich and J. F. Nagle, Correlation between length and tilt of lipid tails, *J. Chem. Phys.* **143**, 154702 (2015).
- [89] H. A. Scheidt, K. Kolocaj, J. Veje Kristensen, D. Huster, and D. Langosch, Transmembrane helix induces membrane fusion through lipid binding and splay, *J. Phys. Chem. Lett.* **9**, 3181 (2018).
- [90] W. Helfrich and J. Prost, Intrinsic bending force in anisotropic membranes made of chiral molecules, *Phys. Rev. A* **38**, 3065 (1988).
- [91] J. B. Fournier and P. Galatola, Bilayer membranes with 2D-nematic order of the surfactant polar heads, *Braz. J. Phys.* **28**, 329 (1998).
- [92] G. Napoli and L. Vergori, Equilibrium of nematic vesicles, *J. Phys. A: Math. Theor.* **43**, 445207 (2010).
- [93] J. A. Santiago, G. Chacón-Acosta, and F. Monroy, Membrane stress and torque induced by Frank’s nematic textures: A geometric perspective using surface-based constraints, *Phys. Rev. E* **100**, 012704 (2019).
- [94] A. M. Lebar, A. Velikonja, P. Kramar, and A. Iglič, Internal configuration and electric potential in planar negatively charged lipid head group region in contact with ionic solution, *Bioelectrochemistry* **111**, 49 (2016).
- [95] E. Gongadze, A. Velikonja, Š. Perutkova, P. Kramar, A. Maček-Lebar, V. Kralj-Iglič, and A. Iglič, Ions and water molecules in an electrolyte solution in contact with charged and dipolar surfaces, *Electrochim. Acta* **126**, 42 (2014).
- [96] L. Fernandez-Puente, I. Bivas, M. D. Mitov, and P. Méléard, Temperature and chain length effects on bending elasticity of phosphatidylcholine bilayers, *Europhys. Lett.* **28**, 181 (1994).
- [97] J. F. Nagle, Experimentally determined tilt and bending moduli of single-component lipid bilayers, *Chem. Phys. Lipids* **205**, 18 (2017).
- [98] B. Sorre, A. Callan-Jones, J. B. Manneville, P. Nassoy, J. F. Joanny, J. Prost, B. Goud, and P. Bassereau, Curvature-driven lipid sorting needs proximity to a demixing point and is aided by proteins, *Proc. Natl. Acad. Sci. USA* **106**, 5622 (2009).
- [99] D. Marsh, Elastic curvature constants of lipid monolayers and bilayers, *Chem. Phys. Lipids* **144**, 146 (2006).
- [100] E. Evans, W. Rawicz, and B. A. Smith, Concluding remarks back to the future: Mechanics and thermodynamics of lipid biomembranes, *Faraday Discuss.* **161**, 591 (2013).
- [101] M. Kaltenecker, J. Kremser, M. P. Frewein, P. Zihlerl, D. J. Bonthuis, and G. Pabst, Intrinsic lipid curvatures of mammalian plasma membrane outer leaflet lipids and ceramides, *Biochim. Biophys. Acta* **1863**, 183709 (2021).
- [102] W. D. Bennett and D. P. Tieleman, Water defect and pore formation in atomistic and coarse-grained lipid membranes: Pushing the limits of coarse graining, *J. Chem. Theory Comput.* **7**, 2981 (2011).
- [103] B. Kollmitzer, P. Heftberger, M. Rappolt, and G. Pabst, Monolayer spontaneous curvature of raft-forming membrane lipids, *Soft Matter* **9**, 10877 (2013).
- [104] S. Leikin, M. M. Kozlov, N. L. Fuller, and R. P. Rand, Measured effects of diacylglycerol on structural and elastic properties of phospholipid membranes, *Biophys. J.* **71**, 2623 (1996).
- [105] A. J. Sodt, R. M. Venable, E. Lyman, and R. W. Pastor, Nonadditive Compositional Curvature Energetics of Lipid Bilayers, *Phys. Rev. Lett.* **117**, 138104 (2016).
- [106] S. R. Lakes, in *The Biomedical Engineering Handbook*, edited by J. D. Bronzino (CRC, Boca Raton, 2006).
- [107] M. M. Kozlov and W. Helfrich, Effects of a cosurfactant on the stretching and bending elasticities of a surfactant monolayer, *Langmuir* **8**, 2792 (1992).
- [108] D. P. Siegel, The Gaussian curvature elastic energy of intermediates in membrane fusion, *Biophys. J.* **95**, 5200 (2008).
- [109] J. L. Symons, K. J. Cho, J. T. Chang, G. Du, M. N. Waxham, J. F. Hancock, I. Levental, and K. R. Levental, Lipidomic atlas of mammalian cell membranes reveals hierarchical variation induced by culture conditions, subcellular membranes, and cell lineages, *Soft Matter* **17**, 288 (2021).
- [110] T. M. Fischer, Bending stiffness of lipid bilayers. III. Gaussian curvature, *J. Phys. (France) II* **2**, 337 (1992).

- [111] T. M. Fischer, Bending stiffness of lipid bilayers. V. Comparison of two formulations, *J. Phys. (France) II* **3**, 1795 (1993).
- [112] T. M. Fischer, Mechanisms for determining the time scales in vesicle budding, *Phys. Rev. E* **50**, 4156 (1994).
- [113] S. Penič, L. Mesarec, M. Fošnarič, L. Mrówczyńska, H. Hägerstrand, V. Kralj-Iglič, and A. Iglič, Budding and fission of membrane vesicles: A mini review, *Front. Phys.* **8**, 342 (2020).
- [114] J. B. Fournier, Nontopological Saddle-Splay and Curvature Instabilities from Anisotropic Membrane Inclusions, *Phys. Rev. Lett.* **76**, 4436 (1996).
- [115] V. Kralj-Iglič, V. Heinrich, S. Svetina, and B. Žekš, Free energy of closed membrane with anisotropic inclusions, *Eur. Phys. J. B* **10**, 5 (1999).
- [116] M. M. Kozlov, S. L. Leikin, and V. S. Markin, Elastic properties of interfaces. Elasticity moduli and spontaneous geometric characteristics, *J. Chem. Soc. Faraday Trans. 2* **85**, 277 (1989).
- [117] M. Deserno, Fluid lipid membranes: From differential geometry to curvature stresses, *Chem. Phys. Lipids* **185**, 11 (2015).
- [118] A. Ben-Shaul, Molecular theory of chain packing, elasticity and lipid-protein interaction in lipid bilayers, in *Structure and Dynamics of Membranes*, edited by R. Lipowsky and E. Sackmann (Elsevier, Amsterdam, 1995), pp. 359–401.
- [119] A. Iglič, B. Babnik, U. Gimsa, and V. Kralj-Iglič, On the role of membrane anisotropy in the beading transition of undulated tubular membrane structures, *J. Phys. A: Math. Gen.* **38**, 8527 (2005).
- [120] A. G. Petrov and I. Bivas, Elastic and flexoelectric aspects of out-of-plane fluctuations in biological and model membranes, *Prog. Surf. Sci.* **16**, 389 (1984).
- [121] K. V. Pinigin, Determination of elastic parameters of lipid membranes with molecular dynamics: A review of approaches and theoretical aspects, *Membranes* **12**, 1149 (2022).
- [122] S. Leibler, Curvature instability in membranes, *J. Phys.* **47**, 507 (1986).
- [123] I. A. Barragán Vidal, C. M. Rosetti, C. Pastorino, and M. Müller, Measuring the composition-curvature coupling in binary lipid membranes by computer simulations, *J. Chem. Phys.* **141**, 194902 (2014).
- [124] R. Goetz and R. Lipowsky, Computer simulations of bilayer membranes: Self-assembly and interfacial tension, *J. Chem. Phys.* **108**, 7397 (1998).
- [125] J. Eid, H. Razmazma, A. Jraj, A. Ebrahimi, and L. Monticelli, On calculating the bending modulus of lipid bilayer membranes from buckling simulations, *J. Phys. Chem. B* **124**, 6299 (2020).
- [126] S. Kawamoto, T. Nakamura, S. O. Nielsen, and W. Shinoda, A guiding potential method for evaluating the bending rigidity of tensionless lipid membranes from molecular simulation, *J. Chem. Phys.* **139**, 034108 (2013).
- [127] V. A. Harmandaris and M. Deserno, A novel method for measuring the bending rigidity of model lipid membranes by simulating tethers, *J. Chem. Phys.* **125**, 204905 (2006).
- [128] G. Bubnis, H. J. Risselada, and H. Grubmüller, Exploiting Lipid Permutation Symmetry to Compute Membrane Remodeling Free Energies, *Phys. Rev. Lett.* **117**, 188102 (2016).
- [129] T. R. Galimzyanov, P. V. Bashkirov, P. S. Blank, J. Zimmerberg, O. V. Batishchev, and S. A. Akimov, Monolayerwise application of linear elasticity theory well describes strongly deformed lipid membranes and the effect of solvent, *Soft Matter* **16**, 1179 (2020).
- [130] K. M. Nakagawa and H. Noguchi, Nonuniqueness of local stress of three-body potentials in molecular simulations, *Phys. Rev. E* **94**, 053304 (2016).
- [131] H. Noguchi, Virtual bending method to calculate bending rigidity, saddle-splay modulus, and spontaneous curvature of thin fluid membranes, *Phys. Rev. E* **102**, 053315 (2020).
- [132] O. Farago and P. Pincus, Statistical mechanics of bilayer membrane with a fixed projected area, *J. Chem. Phys.* **120**, 2934 (2004).
- [133] W. Helfrich and R. M. Servuss, Undulations, steric interaction and cohesion of fluid membranes, *Nuovo Cimento D* **3**, 137 (1984).
- [134] P. I. Kuzmin, S. A. Akimov, Y. A. Chizmadzhev, J. Zimmerberg, and F. S. Cohen, Line tension and interaction energies of membrane rafts calculated from lipid splay and tilt, *Biophys. J.* **88**, 1120 (2005).
- [135] J. B. Klauda, R. M. Venable, J. A. Freites, J. W. O'Connor, D. J. Tobias, C. Mondragon-Ramirez, I. Vorobyov, A. D. Mackerell, Jr., and R. W. Pastor, Update of the CHARMM all-atom additive force field for lipids: Validation on six lipid types, *J. Phys. Chem. B* **114**, 7830 (2010).
- [136] J. Guven, Membrane geometry with auxiliary variables and quadratic constraints, *J. Phys. A: Math. Gen.* **37**, L313 (2004).
- [137] R. Capovilla and J. Guven, Stresses in lipid membranes, *J. Phys. A: Math. Gen.* **35**, 6233 (2002).